NASA/TM-20220007033

Noise Correction for Supersonic Inlet Geometry

David Bruce Stephens
Glenn Research Center, Cleveland, Ohio

November 2022

NASA STI Program . . . in Profile

Since its founding, NASA has been dedicated to the advancement of aeronautics and space science. The NASA Scientific and Technical Information (STI) Program plays a key part in helping NASA maintain this important role.

The NASA STI Program operates under the auspices of the Agency Chief Information Officer. It collects, organizes, provides for archiving, and disseminates NASA's STI. The NASA STI Program provides access to the NASA Technical Report Server—Registered (NTRS Reg) and NASA Technical Report Server—Public (NTRS) thus providing one of the largest collections of aeronautical and space science STI in the world. Results are published in both non-NASA channels and by NASA in the NASA STI Report Series, which includes the following report types:

- TECHNICAL PUBLICATION. Reports of completed research or a major significant phase of research that present the results of NASA programs and include extensive data or theoretical analysis. Includes compilations of significant scientific and technical data and information deemed to be of continuing reference value. NASA counter-part of peer-reviewed formal professional papers, but has less stringent limitations on manuscript length and extent of graphic presentations.

- TECHNICAL MEMORANDUM. Scientific and technical findings that are preliminary or of specialized interest, e.g., "quick-release" reports, working papers, and bibliographies that contain minimal annotation. Does not contain extensive analysis.

- CONTRACTOR REPORT. Scientific and technical findings by NASA-sponsored contractors and grantees.

- CONFERENCE PUBLICATION. Collected papers from scientific and technical conferences, symposia, seminars, or other meetings sponsored or co-sponsored by NASA.

- SPECIAL PUBLICATION. Scientific, technical, or historical information from NASA programs, projects, and missions, often concerned with subjects having substantial public interest.

- TECHNICAL TRANSLATION. English-language translations of foreign scientific and technical material pertinent to NASA's mission.

For more information about the NASA STI program, see the following:

- Access the NASA STI program home page at http://www.sti.nasa.gov

- E-mail your question to help@sti.nasa.gov

- Fax your question to the NASA STI Information Desk at 757-864-6500

- Telephone the NASA STI Information Desk at 757-864-9658

- Write to:
  NASA STI Program
  Mail Stop 148
  NASA Langley Research Center
  Hampton, VA 23681-2199

NASA/TM-20220007033

Noise Correction for Supersonic Inlet Geometry

David Bruce Stephens
Glenn Research Center, Cleveland, Ohio

National Aeronautics and
Space Administration

Glenn Research Center
Cleveland, Ohio 44135

November 2022

Acknowledgments

The NASA Commercial Supersonic Technology Project funded this work with James Bridges as subproject manager for airport noise. Thanks to my colleague Brian Heberling for performing the Reynolds-averaged Navier-Stokes (RANS) calculation using Fluent (Ansys, Inc.).

This work was sponsored by the Advanced Air Vehicle Program
at the NASA Glenn Research Center

Level of Review: This material has been technically reviewed by technical management.

This report is available in electronic form at http://www.sti.nasa.gov/ and http://ntrs.nasa.gov/

Noise Correction for Supersonic Inlet Geometry

David Bruce Stephens
National Aeronautics and Space Administration
Glenn Research Center
Cleveland, Ohio 44135

Summary

Engine inlet geometry for supersonic aircraft is quite different than for subsonic aircraft. The present study considers whether inlet shape has a significant impact on the radiated sound and flyover noise. Axisymmetric two-dimensional simulations were performed for both subsonic and supersonic inlet geometries with the same acoustic input. The effect in the far field is complicated but overall impact on flyover noise from the effective perceived noise level (EPNL) metric was found to be only about 0.5 dB.

1.0 Introduction

Predicting noise for concept aircraft at the early stages of design typically relies on using empirical models for the fan noise source. These models are most accurate when used to interpolate within the range of configurations they were developed from. Inlet shape is not typically considered when using the models for subsonic aircraft, but an efficient supersonic inlet has a significantly different shape. The supersonic inlet used in the present study was modified from the nonproprietary inlet for the LM1044 concept aircraft (Ref. 1). This inlet is an axisymmetric spike designed for a Mach 1.7 flight speed. This inlet utilizes a sliding cowl that exposes an auxiliary inlet idealized as an axisymmetric slot. The auxiliary inlet provides additional airflow into the engine when the aircraft is operating at low flight speeds, such as during landing and takeoff. Heath, Seidel, and Rallabhandi found that an auxiliary inlet should remain open up to Mach 0.6 (Ref. 2). The present work assumes that the auxiliary inlet will be open during community noise certification. An example of a conventional subsonic inlet and a supersonic axial spike inlet with auxiliary inlet is shown in Figure 1.

Data for empirical fan noise models is typically obtained from engines on a test stand, although wind tunnel data can also be used. On a test stand, the engine is stationary with respect to the surrounding air in a so-called static condition. A special inlet design is often used, which is different from the “flight” inlet that would be used for an engine mounted on an aircraft. The static inlet is designed to provide clean

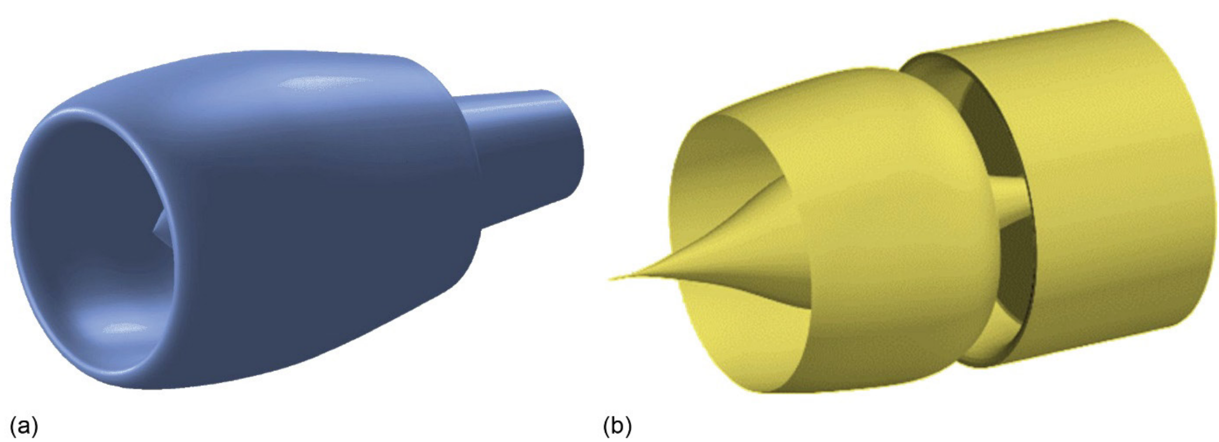

Figure 1.—Inlets. (a) Subsonic. (b) Supersonic.

inflow to the engine under this stationary condition. Sometimes a bellmouth inlet is used, but flight-like inlets are also employed. Pictures and discussion of the acoustic impact of a static inlet and flight inlet are given by Silcox (Ref. 3). In addition to the geometric shape of an inlet used for a test, an inlet control screen device is often used to break up turbulence and eliminate ground effects, although this is not part of the present study. An engine for a supersonic aircraft would be similarly tested on a stand with a static-type inlet that would be completely different from the inlet designed for supersonic flight. In a wind tunnel, a flight inlet can be used since the wind tunnel will provide the simulated forward motion required to set the proper streamlines, fan-face conditions, and turbulence cleanup.

The shape of the inlet will affect both the airflow into the engine and the sound radiation from the engine upstream through the inlet. A number of supersonic inlet designs are described by Slater (Ref. 4), but the present report will focus on the axisymmetric spike type, as shown in Figure 1. The goal of this effort is to propose a methodology for a correction that can be applied to engine noise predictions, enabling the empirical models developed using subsonic designs to be applied to supersonic aircraft noise predictions. The method used to develop the correction will also be documented, as other inlet designs will require a different correction. The present work does not consider the modification of the fan noise source due to the inlet geometry, which would require a turbomachinery simulation.

The outline of the present report is as follows. Section 2.0 reviews the existing empirical fan models and some fan noise propagation literature. Then a methodology for using computational acoustic tools to simulate inlet radiated noise is described in Section 3.0. A series of investigations about different parameters that affect the results are documented in Section 4.0. A correction method for empirical fan noise models is given in Section 5.0 and applied to flyover noise in Section 6.0. The last section provides a summary and conclusions.

2.0 Literature Review

Two empirical fan noise model frameworks have been developed by NASA. Both are available as part of the NASA Aircraft Noise Prediction Program (ANOPP) 2 (Ref. 5). The Heidmann and F120 fan models are discussed in Reference 5, sections 811 and 813, respectively. A brief review and comparison is provided here, along with a short review of previous studies on duct acoustics as it relates to inlet radiated fan noise.

2.1 Heidmann Fan Model

The Heidmann fan noise model framework was developed by Marcus Heidmann at NASA Lewis (now Glenn) Research Center based on data acquired from a full-scale outdoor fan rig (Ref. 6). This is the original model, denoted method 1 in Reference 5. Method 2 by AlliedSignal Engines (now Honeywell Aerospace) is intended for small fans (Ref. 7). Method 3 is by GE Aircraft Engines (now GE Aviation) and is fit to data from large fans (Ref. 8). Method 4 is based on the NASA Source Diagnostic Test (SDT) fan (Ref. 9). Users must pick which method is most appropriate for the fan they are modeling.

The Heidmann method models utilize relatively simple functional expressions to incorporate the various aspects of fan noise. The sound pressure level (SPL) is given as an independent function of frequency and directivity. Equation (1) demonstrates the framework:

$$\mathrm{SPL}(f,\theta) = A\left(\Delta T^{*}, M_r, \ldots\right) + F(f) + D(\theta) \tag{1}$$

where the amplitude function A is dependent on parameters such as the temperature rise generated by the fan ΔT^{*}, the tip relative Mach number M_r, and the rotor-stator spacing. The term $F(f)$ is a tabulated function of frequency, and $D(\theta)$ provides the directivity dependence of the spectrum.

The directivity term $D(\theta)$ is provided as a different set of values for the four versions of the fan model and for the three types of fan noise predicted. Figure 2 shows the function $D(\theta)$ for the inlet radiated tone noise, Figure 3 is the inlet broadband directivity, and Figure 4 is the multiple pure tone (MPT) noise directivity. The tone and broadband noise peak at around 30° from upstream but note that the data tables are only provided at increments of 10°.

The MPT directivity peaks at higher angles than the other inlet sources due to its higher propagation angle in the duct sound field. MPT noise is caused by irregularities in the shockwaves from a fan with a supersonic tip speed (Ref. 10). A recent review of model fan data from wind tunnel tests suggests that improved manufacturing methods result in fairly little MPT noise (Ref. 11), and thus, this sound source will be neglected in the present study. The two remaining noise sources in the Heidmann fan model are inlet tone and broadband components, largely produced by rotor-stator interaction and “rotor alone” sources.

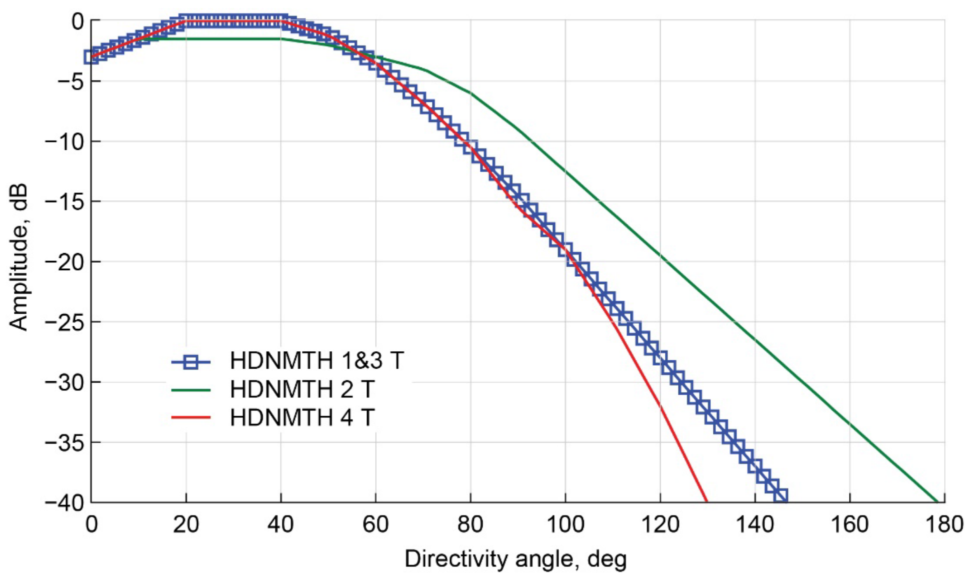

Figure 2.—Directivity function for Heidmann model inlet tone noise.

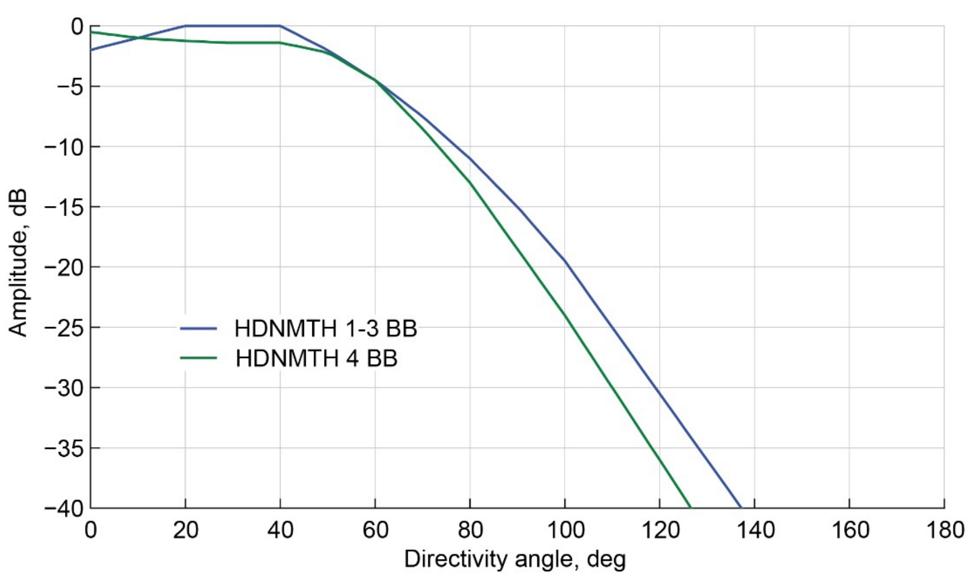

Figure 3.—Directivity function for Heidmann model inlet broadband noise.

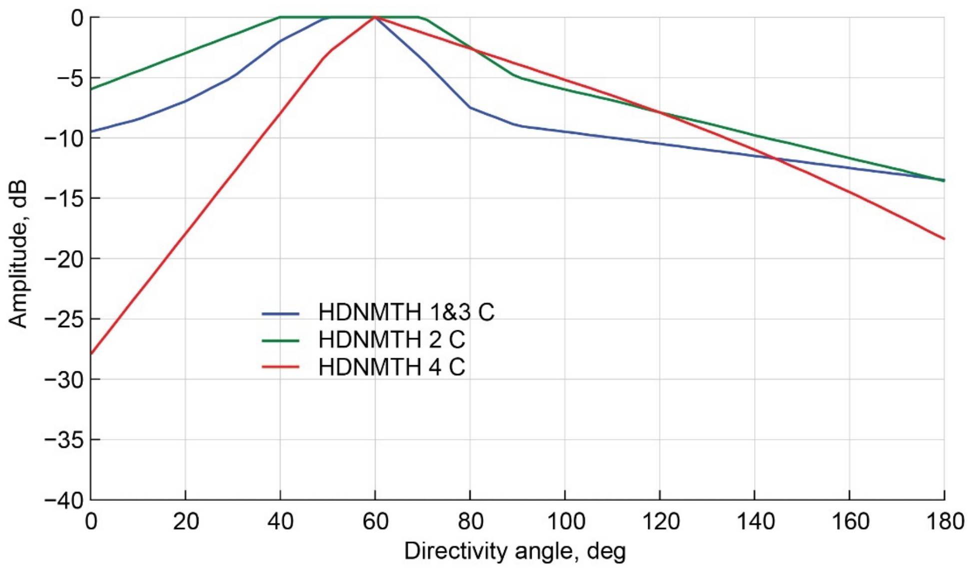

Figure 4.—Directivity function for Heidmann model inlet multiple pure tone (MPT) noise.

Methods 1 to 3 include a flag for the presence of inlet guide vanes (IGVs) that affect the blade passing frequency (BPF) tone level. Modern subsonic engines do not utilize IGVs, but supersonic military engines often use them. It is unclear if commercial supersonic engines will use them or not.

2.2 HSRNoise Fan Model

The F120 fan model (Ref. 12) is an alternative to the Heidmann method models and may be particularly well suited to predicting fan noise for a high-pressure-ratio supersonic engine. It was developed during the NASA High-Speed Research (HSR) program and is based on test data from a single engine with a three-stage fan tested on a stand with a bellmouth inlet. The only inputs to the model are fan hub and tip diameter, fan speed, and fan blade count. While the input is simpler than for Heidmann, the spectral directivity for tone and broadband are both dependent on *Ustar*, which is a dimensionless fan tip speed parameter (Figure 5 shows the F120 fan model tone directivity, and Figure 6 shows the broadband directivity).

As part of the HSR program, research was conducted into the effect of inlet geometry on the fan noise. This included several studies at Virginia Tech (Refs. 13 and 14) and an investigation at the Boeing Low-Speed Aeroacoustic Facility (LSAF) (Ref. 12), which was used to develop a correction for a two-dimensional (2D) bifurcated inlet. Discussion in the report is brief, but the corrections are rather elaborate, giving a frequency- and directivity-dependent curve for broadband noise. Four corrections are available for the three aircraft noise rating conditions of sideline, approach, and flyover, which HSRNoise calls centerline. The centerline correction is provided both with the auxiliary inlet doors open and closed. The disposition of the doors for the other two cases is not clear. The four sets of results are plotted in Figure 7 to Figure 10. Since these corrections were developed with a fan model, they include the effect of the inlet geometry and resulting flow distortion on the fan source.

Tone corrections are provided in Section 3.6 of the HSRNoise report (Ref. 12) for the 2D bifurcated inlet. These are third-order polynomial fits to directivity angle only, with frequency handled by using a separate fit for each of the first four harmonics of the BPF. Of the three aircraft noise rating conditions, only corrections for flyover and approach are provided, shown in Figure 11 to Figure 14.

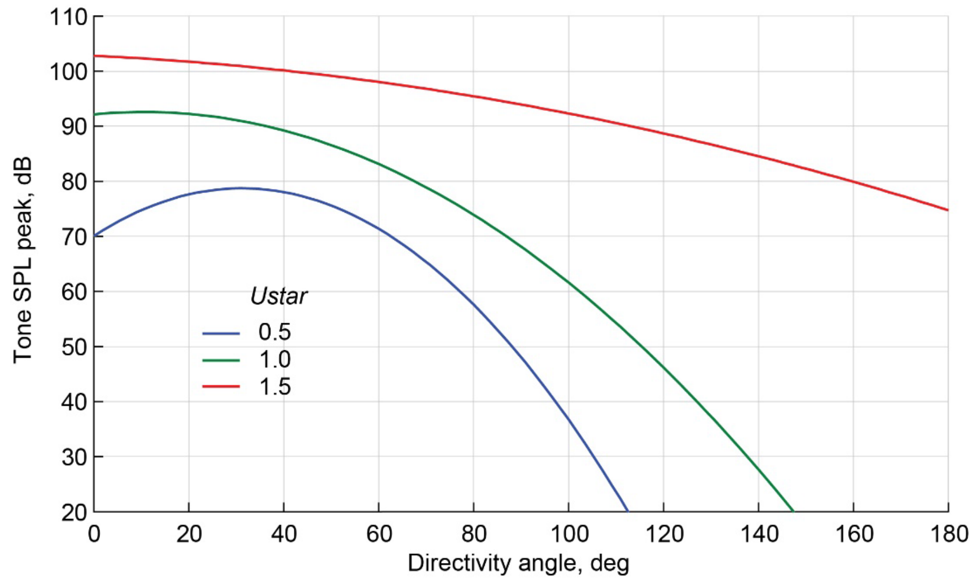

Figure 5.—F120 fan model tone directivity. Sound pressure level (SPL).

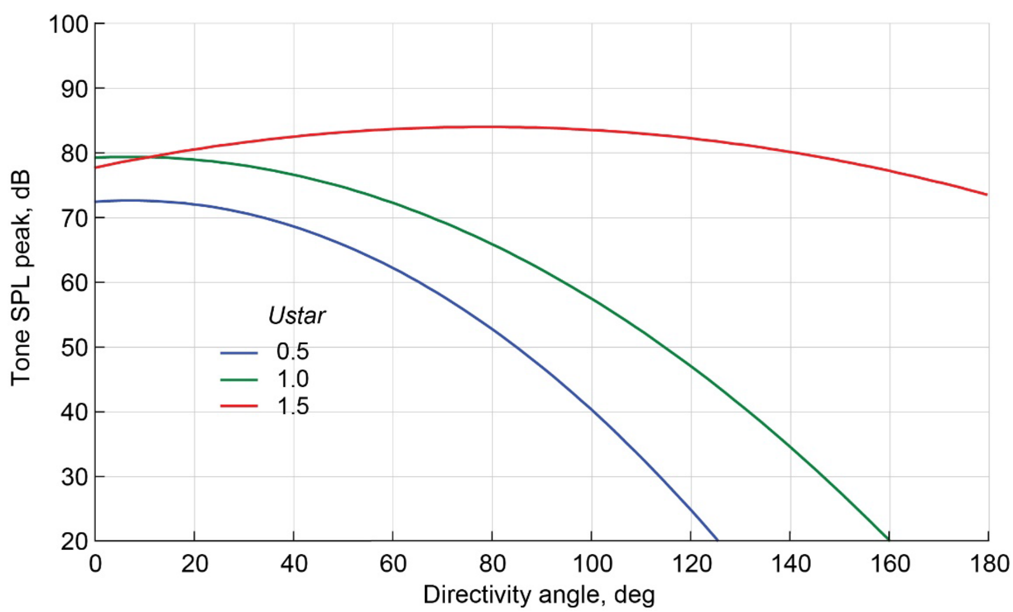

Figure 6.—F120 fan model broadband directivity. Sound pressure level (SPL).

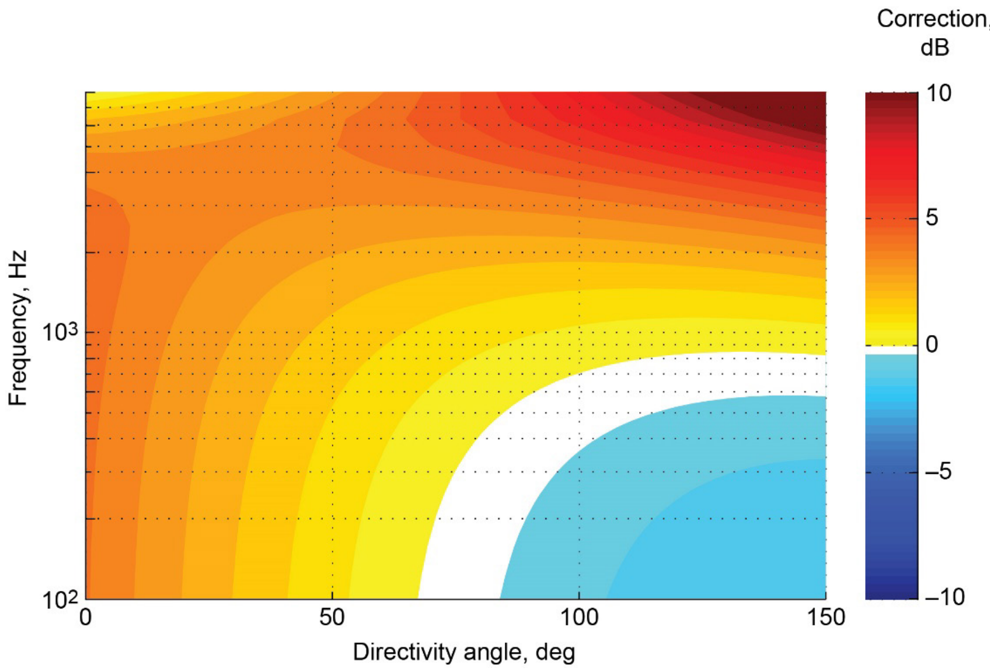

Figure 7.—HSRNoise broadband correction for bifurcated inlet geometry at sideline operating condition.

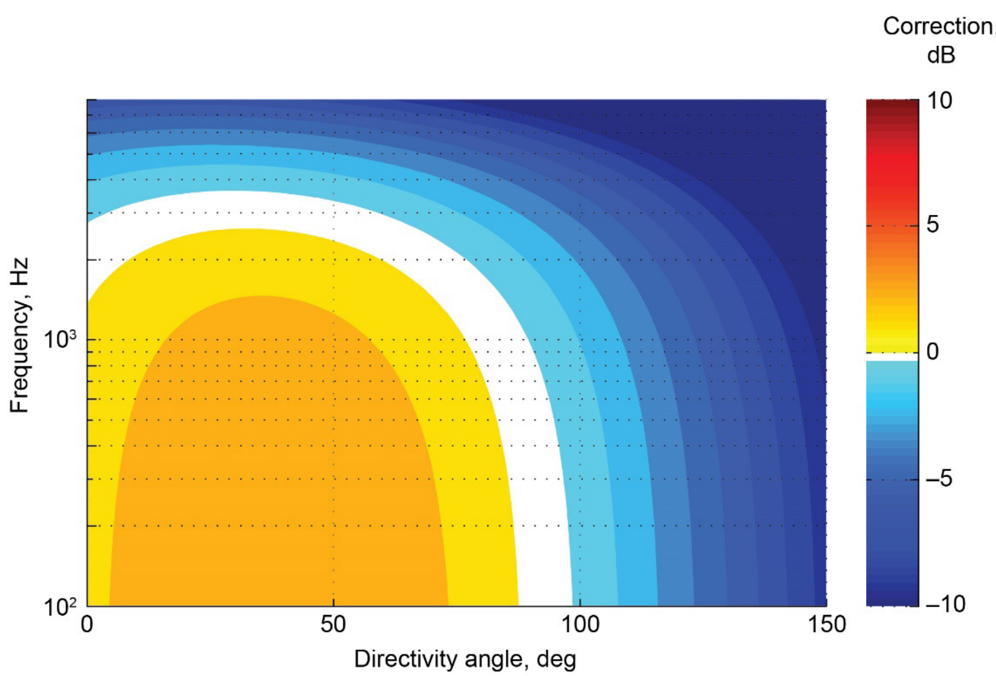

Figure 8.—HSRNoise broadband correction for bifurcated inlet geometry at approach operating condition.

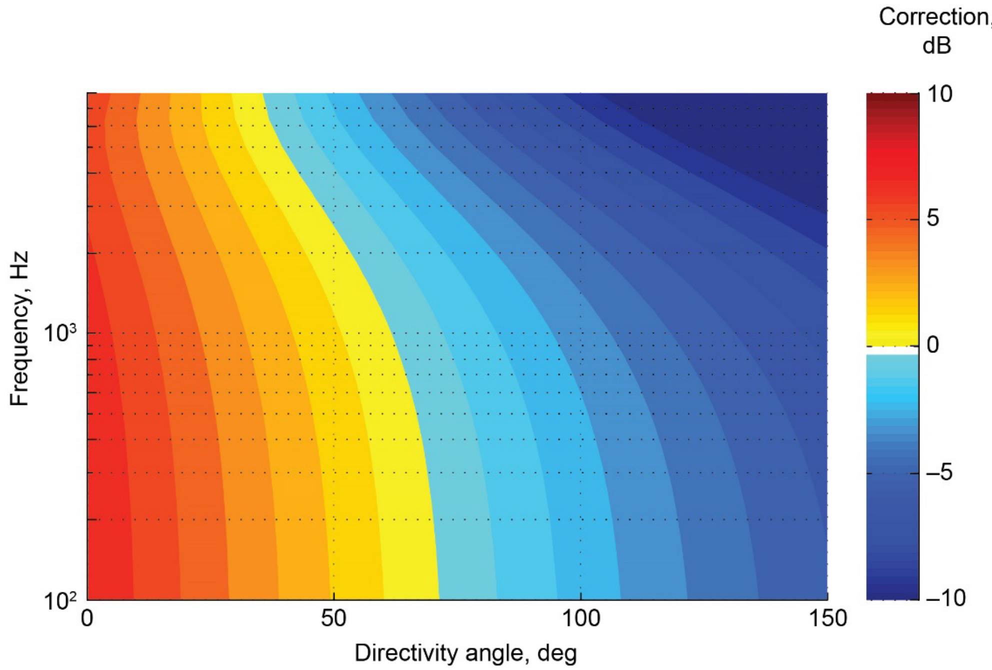

Figure 9.—HSRNoise broadband correction for bifurcated inlet geometry at centerline operating condition with doors closed.

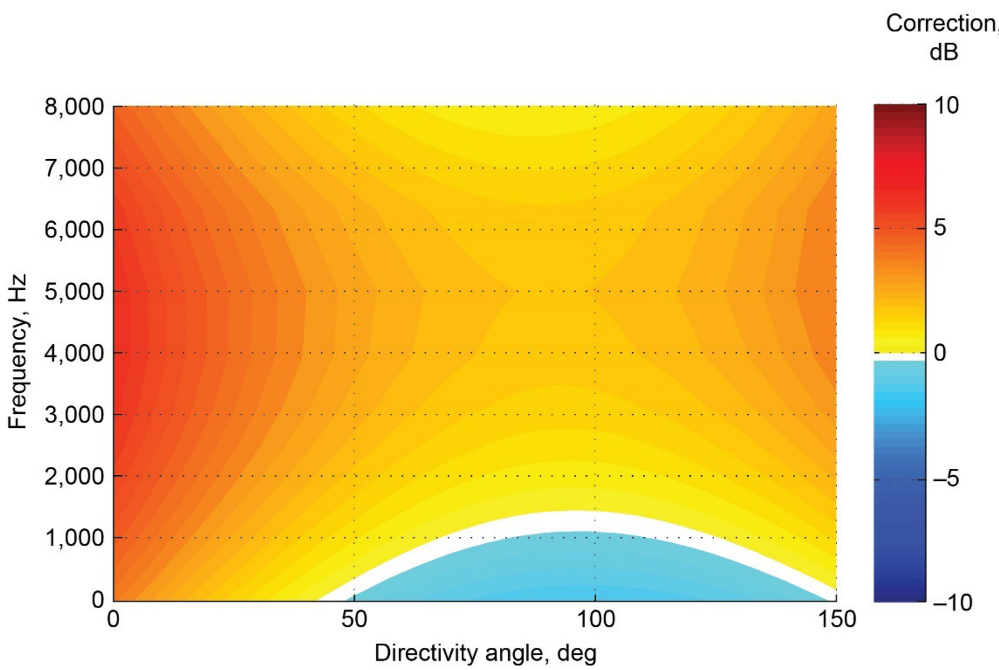

Figure 10.—HSRNoise broadband correction for bifurcated inlet geometry at centerline operating condition with doors open.

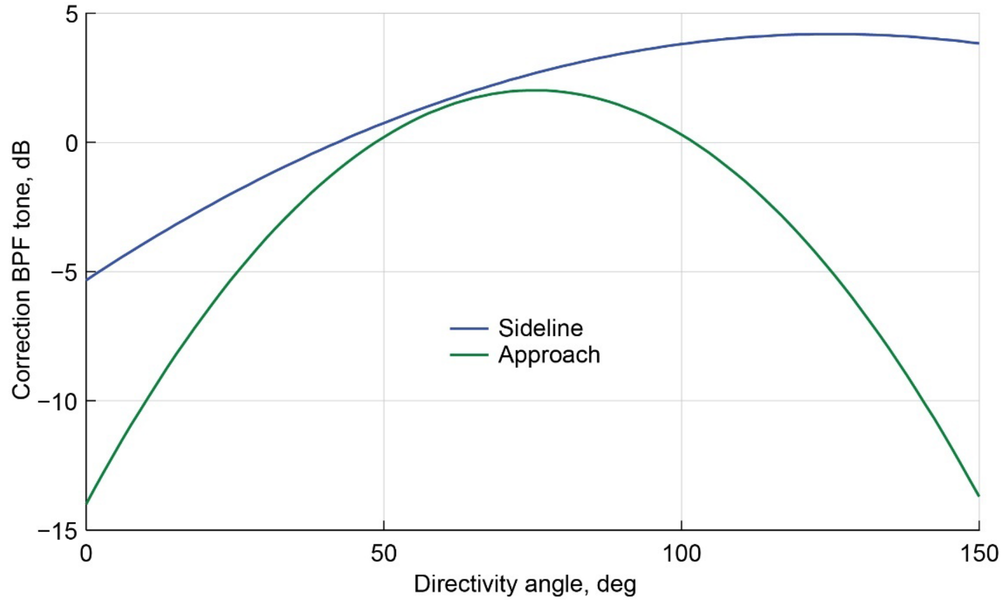

Figure 11.—HSRNoise tone correction for centerline condition with doors open, first harmonic. Blade passing frequency (BPF).

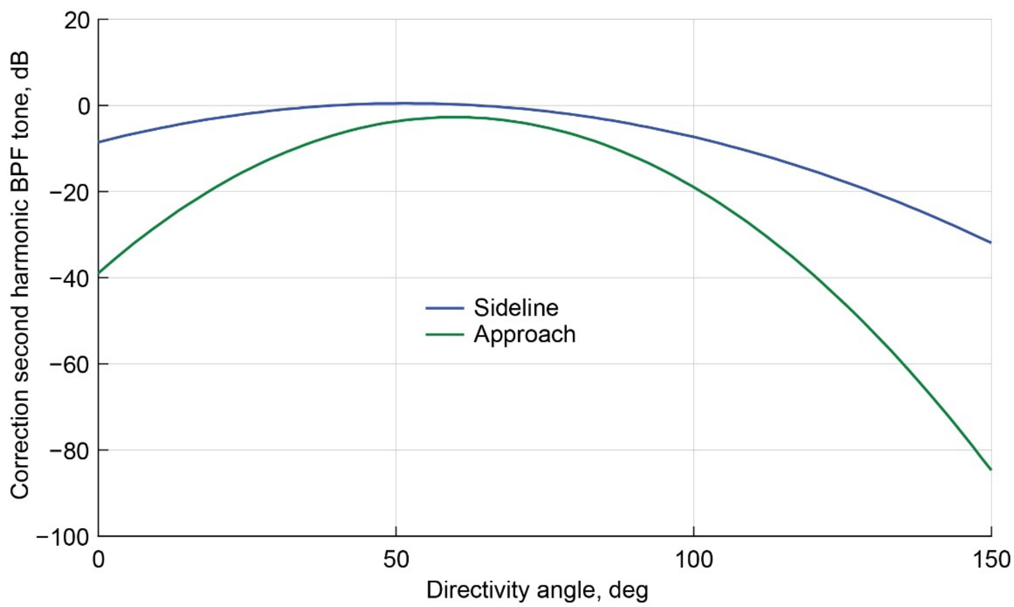

Figure 12.—HSRNoise tone correction for centerline condition with doors open, second harmonic. Blade passing frequency (BPF).

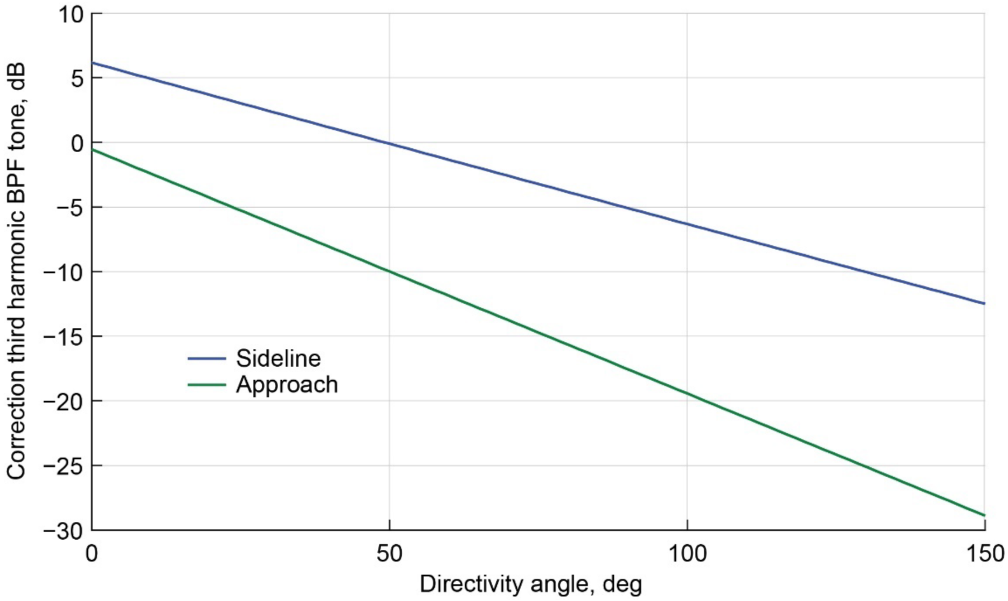

Figure 13.—HSRNoise tone correction for centerline condition with doors open, third harmonic. Blade passing frequency (BPF).

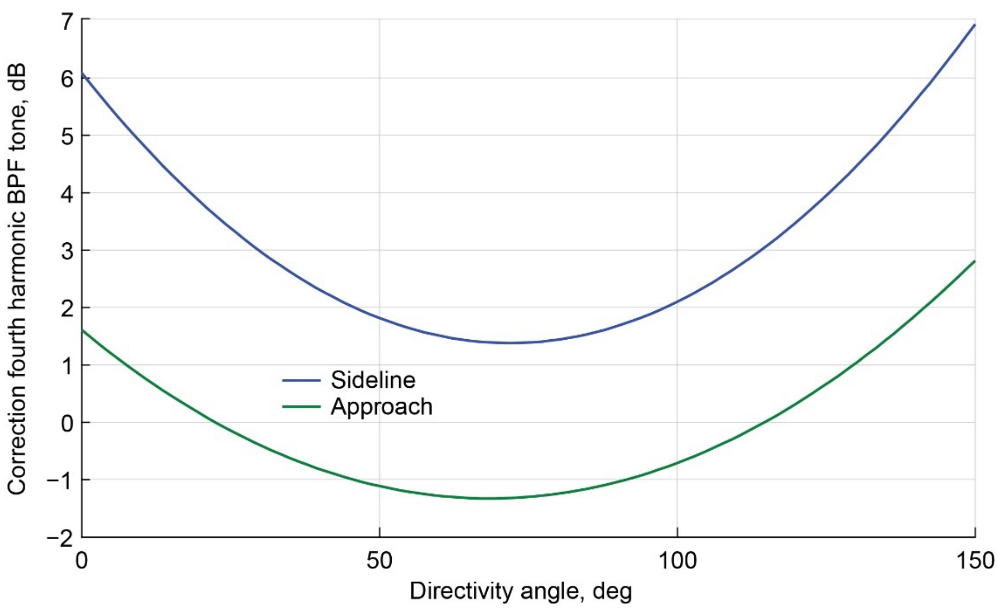

Figure 14.—HSRNoise tone correction for centerline condition with doors open, fourth harmonic. Blade passing frequency (BPF).

2.3 Fan Duct Acoustics Review

Inlet radiated fan noise is a well-developed topic and only a fraction of the relevant papers will be summarized here.

Rice developed an approximate expression for the radiation directivity of duct modes from a circular flanged duct without flow (Ref. 15). Approximations for the Bessel equations were used. It was shown that the radiation pattern was only dependent on the mode cutoff ratio, such that different modes with the same cutoff ratio would have the same far-field directivity. Comparison with fan data showed that the directivity prediction matched broadband noise radiation patterns reasonably well when the predicted modes all had equal energy. This supports the idea of using a simple correction like the one proposed here for broadband noise.

Rice, Heidmann, and Sofrin expanded on the analytical investigation of cylindrical duct modes, this time with uniform internal and external flow (Ref. 16). Eversman developed a finite element tool for acoustic propagation that handles soft-wall conditions and potential flow (Ref. 17). Nallasamy provides a review of these publications and other literature (Ref. 18).

A recent study by Han et al. reviewed sources of MPT noise and simulated propagation through a subsonic inlet using Actran TM (Hexagon AB) (Ref. 19). They compared 2D axisymmetric and three-dimensional (3D) simulations and concluded for the fidelity of the other steps in the process, the 3D model might be unnecessarily complex. A similar reasoning is employed in the present work.

The modal content of a two-stage fan with IGVs would be much richer than a typical single-stage fan, as there are a lot of interactions that lead to Tyler-Sofrin modes (Ref. 20). Additionally, the large number of blade rows will require close spacing to avoid very long engine lengths. These two features are likely to lead to strong modal content in the fan noise propagating in the duct.

3.0 Inlet Simulation Workflow

The main tool for the present study was the Actran TM (Ref. 21) module, which includes tools and workflows designed for 2D axisymmetric sound propagation through subsonic aircraft engine inlets with internal and external flow. The acoustic propagation through a moving media is solved using the Mohring analogy (Ref. 22), which is the Navier-Stokes equations written as a wave operator on enthalpy. This is valid for propagating sound through a flow field that is reversible, adiabatic, and irrotational. A compatible flow field can be generated by the built-in inviscid compressible flow solver. This flow solution will not give rise to any boundary layers, shear layers, or wakes. The validity of using this flow solution for the axisymmetric spike inlet with auxiliary inlet will be investigated.

3.1 Inlet Geometries

The subsonic inlet shown in Figure 1 and used in this study is adapted from the NASA/GE SDT (Ref. 23) geometry. The SDT inlet was for a 0.56-m- (22-in.-) diameter subscale model fan while the LM1044 inlet was full size for a 1.65-m- (65-in.-) diameter fan. The SDT inlet geometry was increased in scale to match the fan-face outer diameters. The inner diameter of the SDT inlet was then slightly larger than the inner diameter of the LM1044 inlet centerbody, so the SDT spinner was scaled down in the radial direction, with a final size of 0.38-m (15-in.) diameter. Some dimensions are given in Figure 15. The origin of this domain was set at the center of the front plane of the inlet.

A 2D slice through the LM1044 inlet was used to generate a computational domain for the present simulations. A circular arc of radius 4 m was centered around a point 1.5 m in front of the engine. This point was chosen as roughly midway between the front and side inlets. Some dimensions are given in Figure 16.

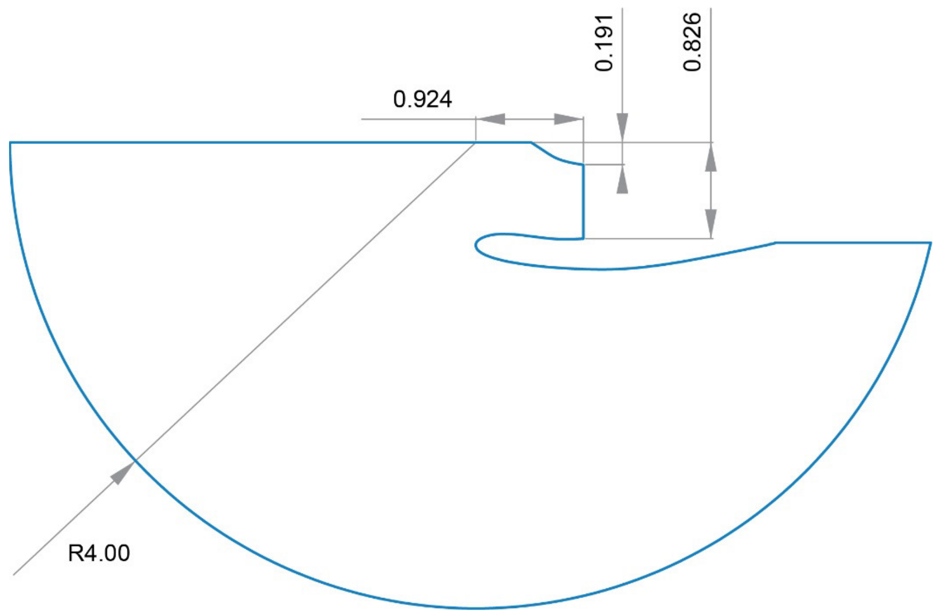

Figure 15.—Basic dimensions for subsonic inlet used in present study. Units are in meters.

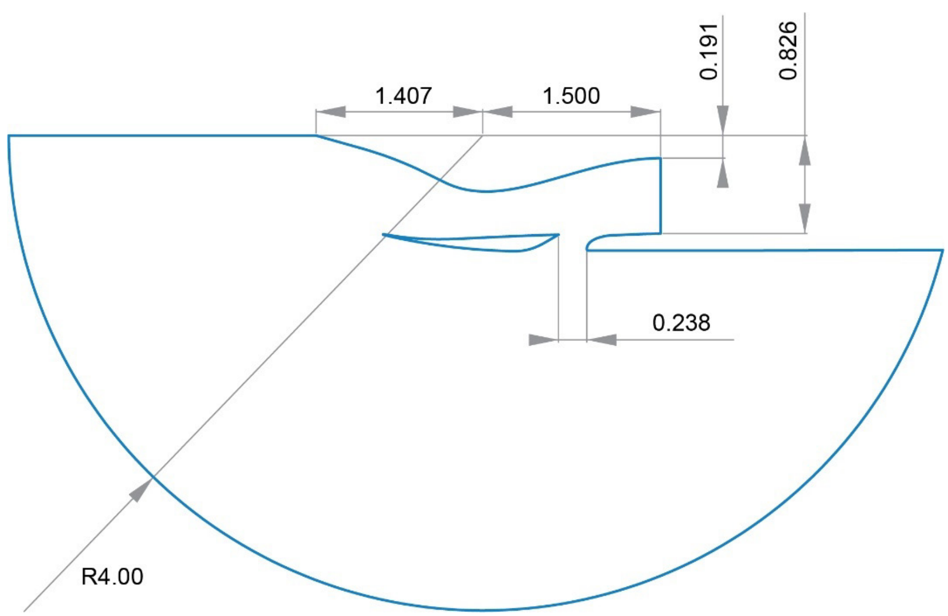

Figure 16.—Basic dimensions for supersonic inlet used in present study. Units are in meters.

3.2 Example Simulation

Actran implements "infinite elements" as a way to handle a nonreflection boundary condition. This also enables acoustic propagation to points in a free field outside the finite element domain in the presence of uniform flow. In the present study, the 4-m-radius arc (shown in Figure 15 and Figure 16) is the infinite element boundary. This handles the outgoing acoustic radiation, and "field points" (virtual microphones) can be placed outside the finite element domain. As shown in Figure 17, the field points used here are on a 46-m (150-ft) arc, distributed from 0° upstream to 150° downstream. This method was used to collect all the directivity data presented in this report.

3.3 Flow Fields

The flow field for the subsonic inlet is shown in Figure 18, while the supersonic inlet flow field is in Figure 19. The free-stream flight speed is 100 m/s, and the fan-face Mach is 180 m/s. These values are derived from Figure 38 of Reference 1, which identified a Mach 0.3 flight speed and a Mach 0.53 fan-face speed. The throat of the subsonic inlet leads to a local region of high-speed flow. This flow field is somewhat similar to that of the flow through the auxiliary inlet slot in the supersonic inlet.

3.4 Sound Fields

An illustration of propagation differences between the two geometries comes from using the same noise input. A hypothetical BPF tone of 2,080 Hz and duct mode $m = 10$, $n = 0$ was used for these investigations, where m is the azimuthal mode number and n is the radial (note that Actran numbers radial modes starting at 1 rather than 0). The duct mode was assigned a unit value of 1 Pa since the corrections will be calculated as differences rather than using absolute values. Figure 20 and Figure 21 show this mode for both inlets and the incompressible flow field.

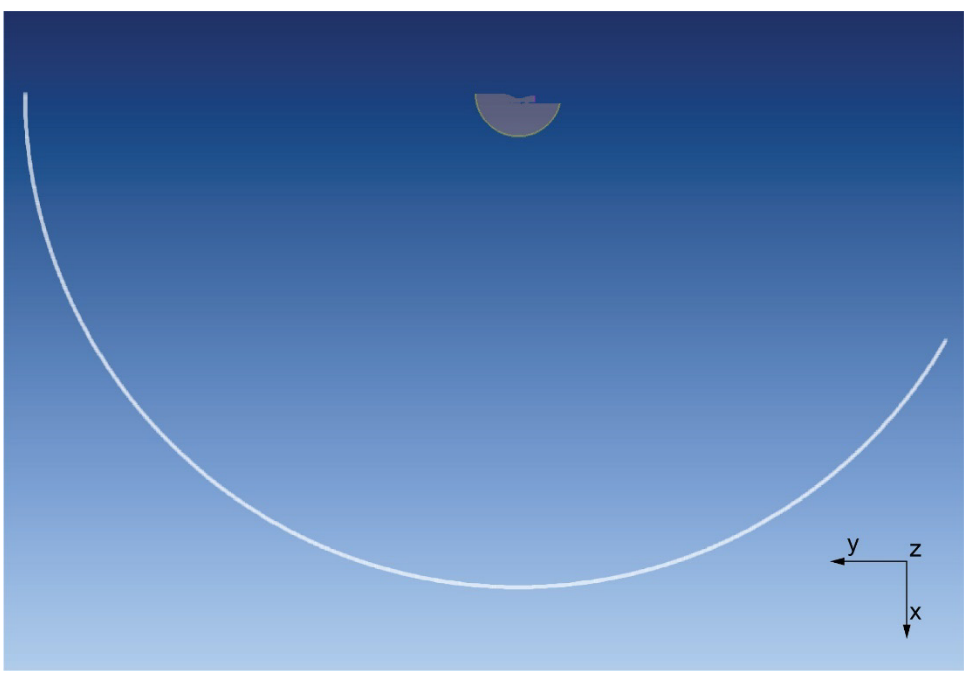

Figure 17.—Finite element domain and virtual microphones.

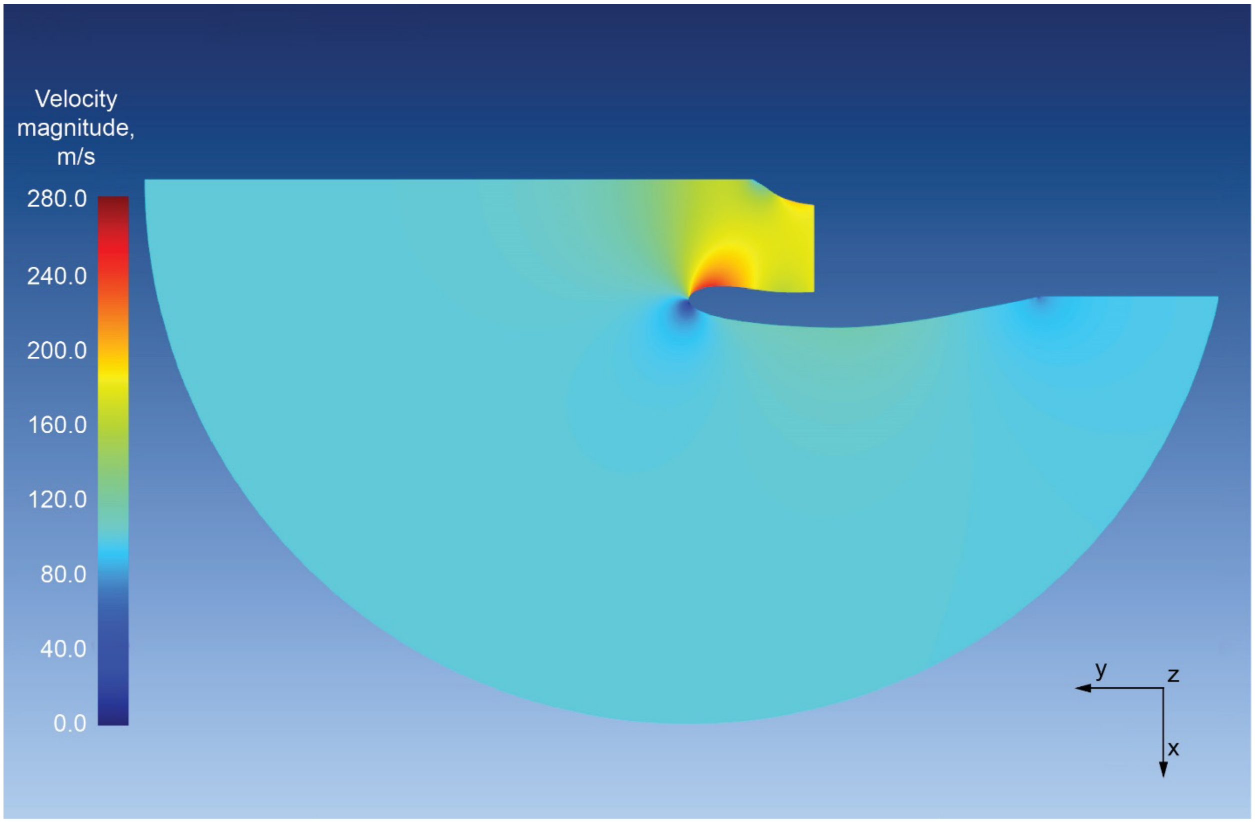

Figure 18.—Flow field for subsonic inlet geometry, 180 m/s fan-face flow, 100 m/s external.

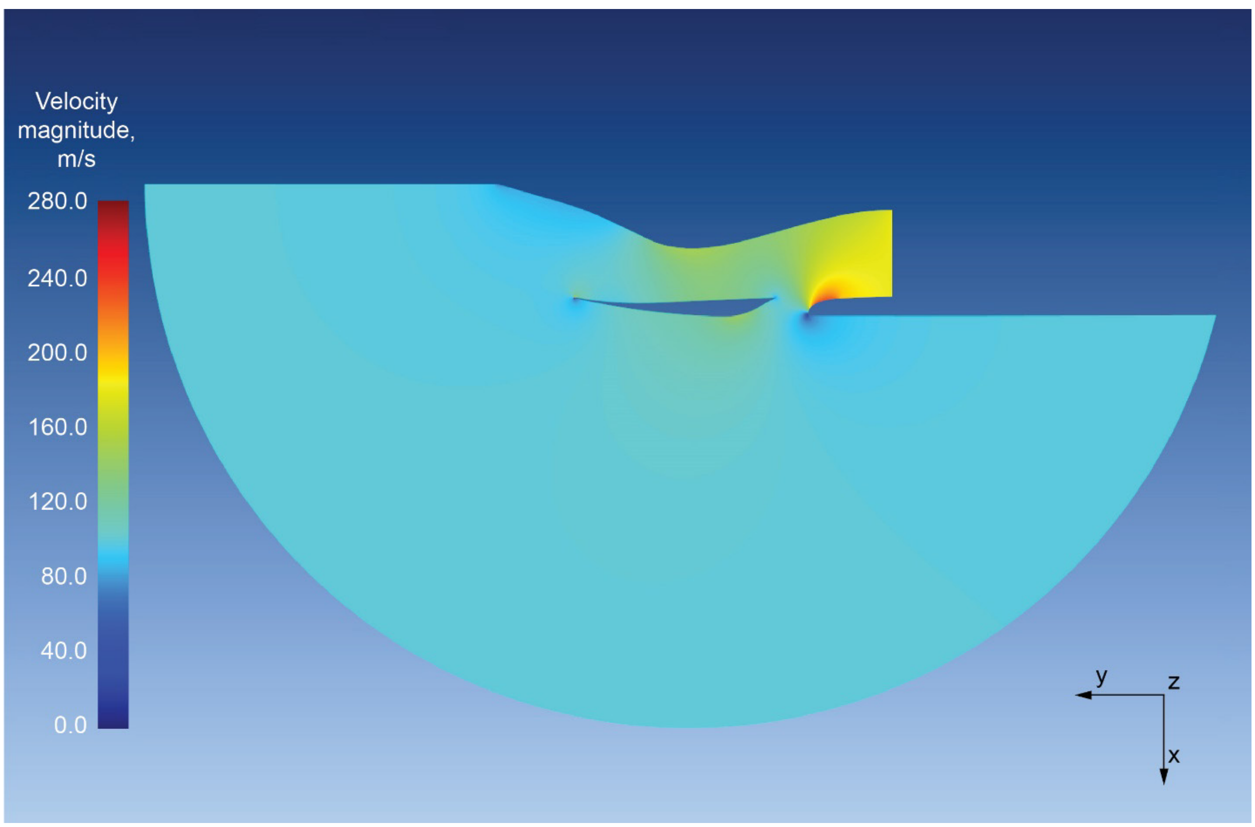

Figure 19.—Flow field for supersonic inlet geometry, 180 m/s fan-face flow, 100 m/s external.

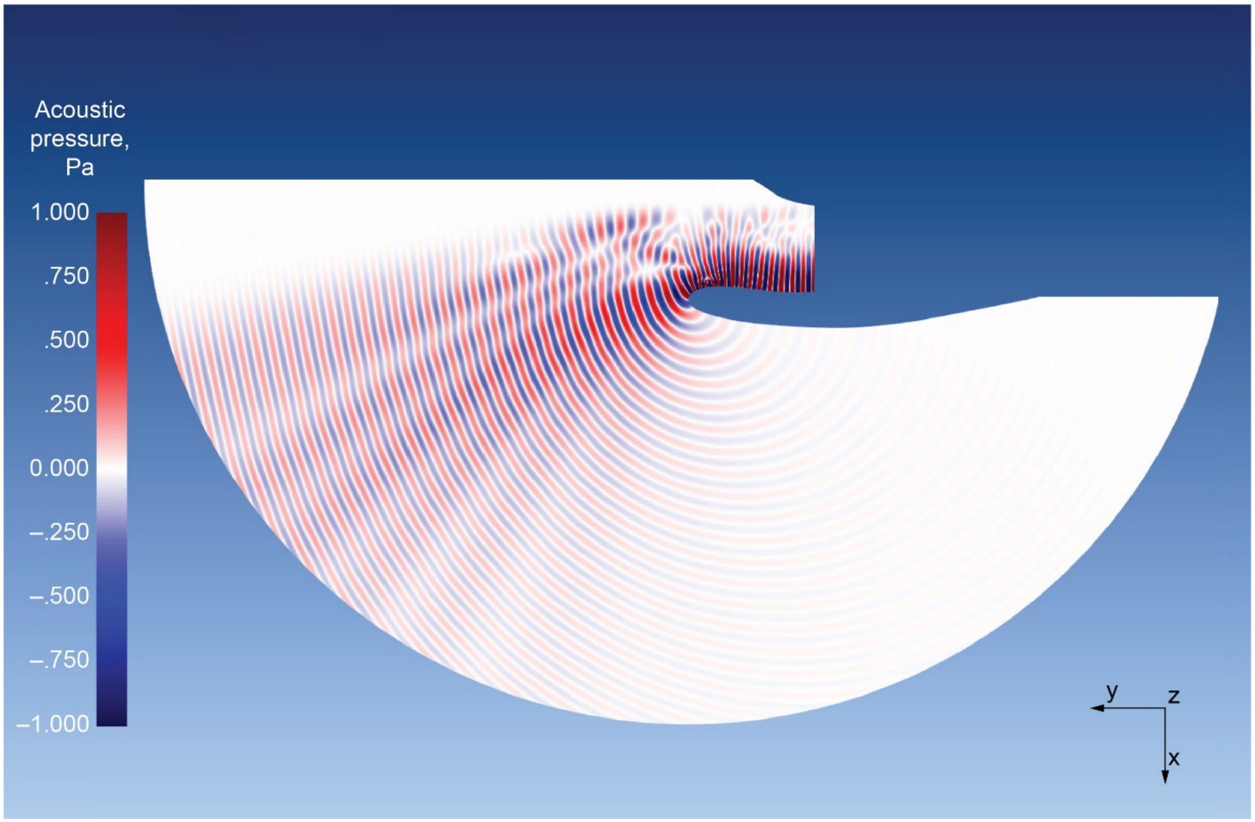

Figure 20.—Sound field for subsonic inlet geometry, 180 m/s fan-face flow, 100 m/s external.

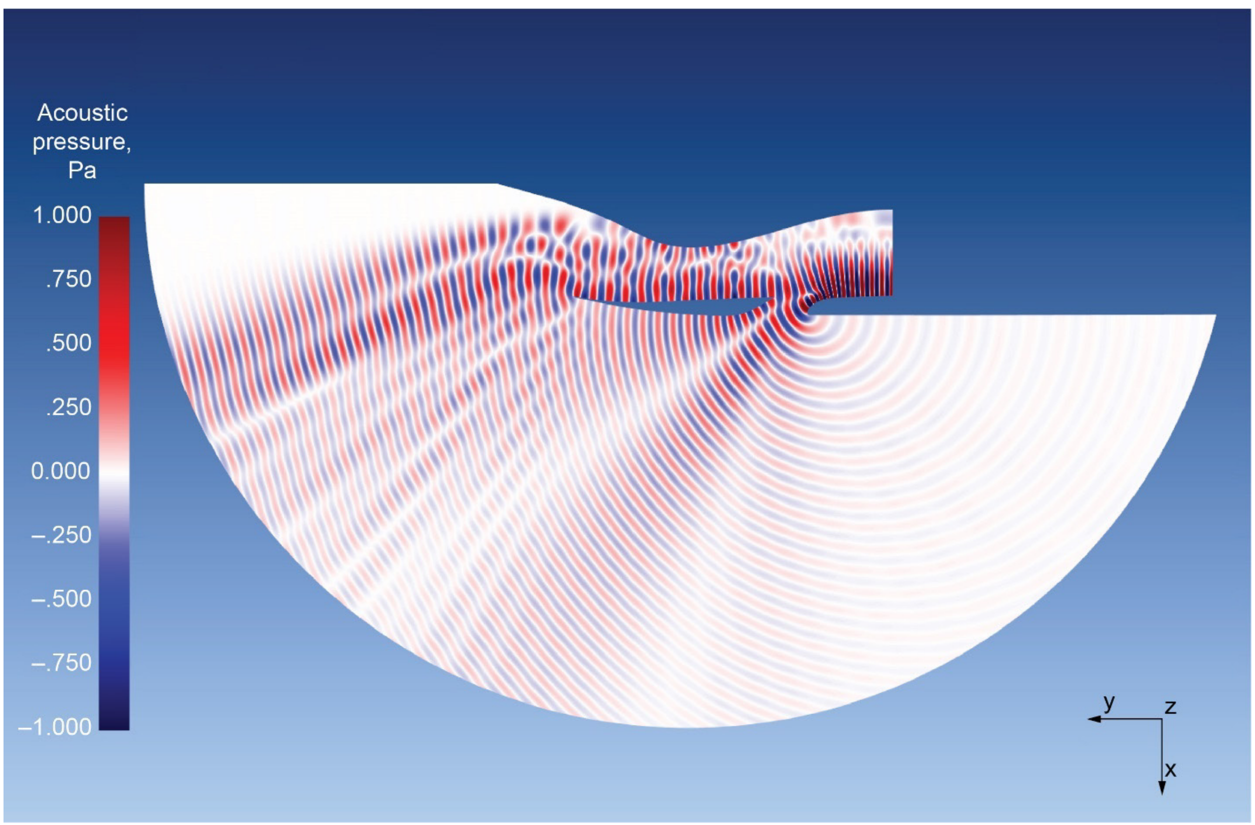

Figure 21.—Sound field for supersonic inlet geometry, 180 m/s fan-face flow, 100 m/s external.

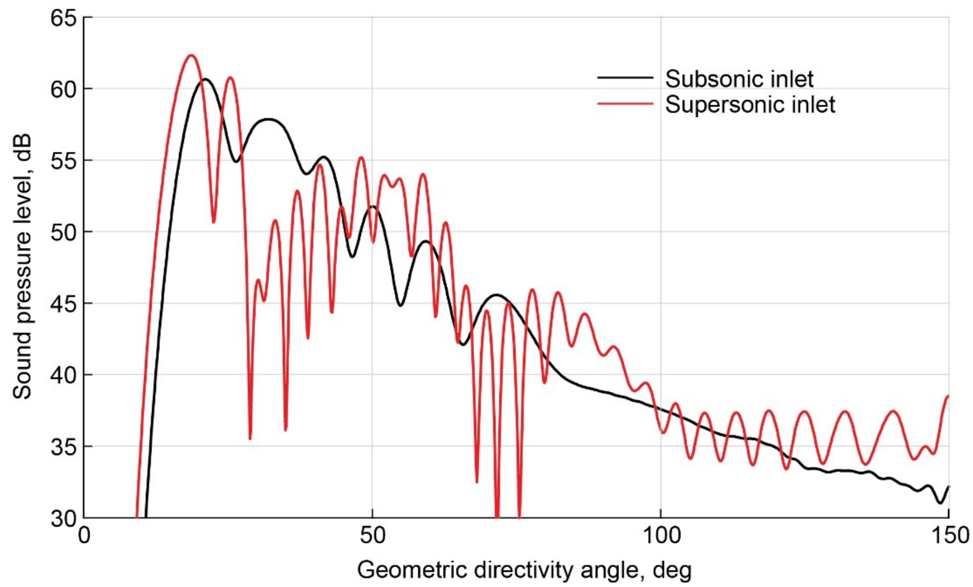

Figure 22.—Example directivity corresponding to Figure 20 and Figure 21.

The compression of the upstream traveling waves due to the fan-face flow is evident. The boundary condition is for a straight annular duct with plug flow, but both inlets feature some flow nonuniformity and changing duct diameters. These effects cause some scattering into radial modes besides the single-mode boundary condition. The high-speed flow around the inlet lip also causes compression of the sound waves. The subsonic inlet has a large main lobe, while the supersonic inlet looks like a two-port system interference pattern with two main lobes and a node in between.

3.5 Sound Directivity

The far-field directivity for these cases is given in Figure 22. The subsonic inlet features a main lobe radiating at 20°. With the supersonic inlet, the sound also has a front lobe between 15° and 25°, with a node in between. The supersonic inlet directivity also has a major forward node at 30°. The subsonic inlet directivity also has many more ripples.

4.0 Results

With a working simulation method demonstrated, a series of studies were conducted to investigate which aspects affect the results. First, the effect of the fan-face flow speed was studied in order to understand how sensitive the radiated noise was to the engine operating condition. Secondly, the radiated sound obtained with an inviscid flow field was compared with that from a viscous solution, which is more computationally expensive to generate. Then the sound power balance is considered, to see if trends about how the noise is radiated from a two-port inlet could be identified. Then some improvements to the simulation method are recorded for future work.

4.1 Effect of Duct Mach Number

The sensitivity of the radiated sound directivity to the flow field in the duct was investigated by varying the fan-face Mach number. Both inlet geometries were considered with fan-face velocities between 160 and 200 m/s. This corresponds to Mach numbers between 0.47 and 0.59. A sample of the flow fields is shown in Figure 23 to Figure 26.

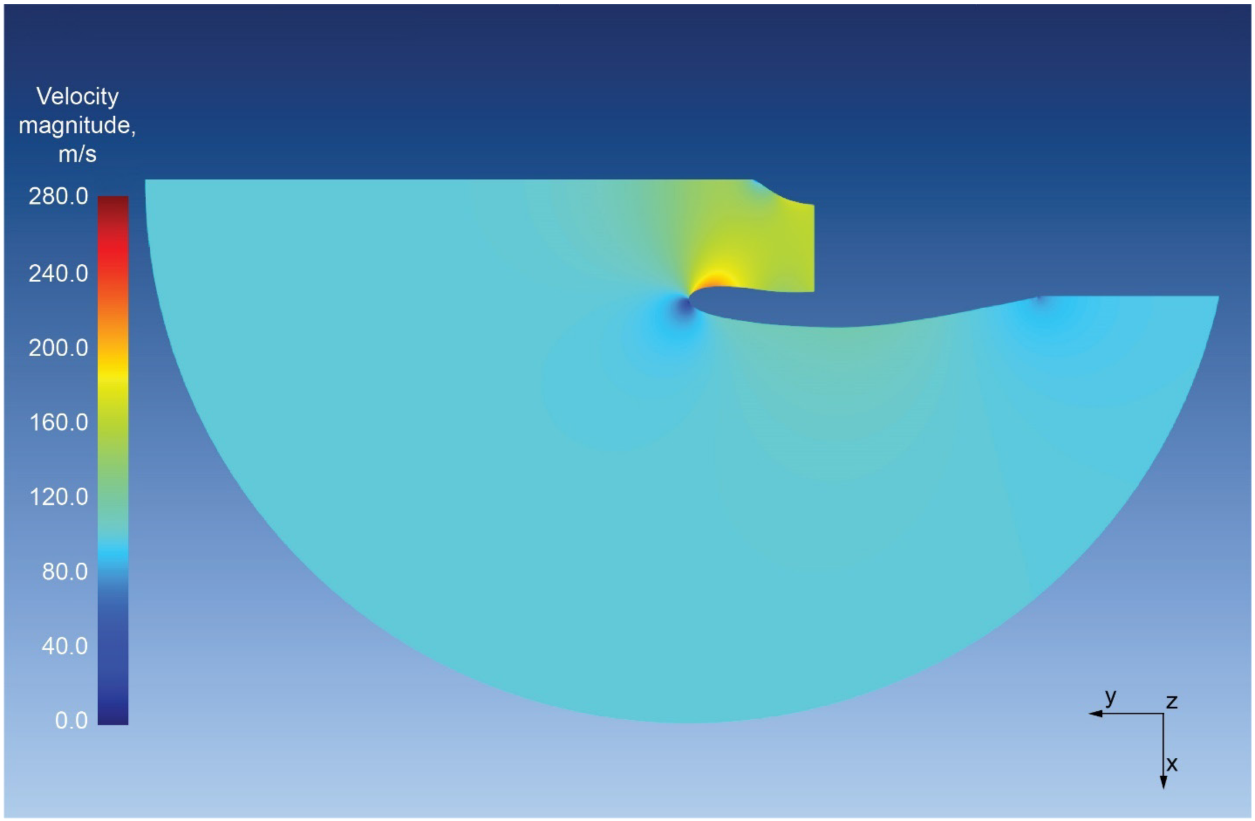

Figure 23.—Flow field for subsonic inlet with 160 m/s fan-face flow, 100 m/s external.

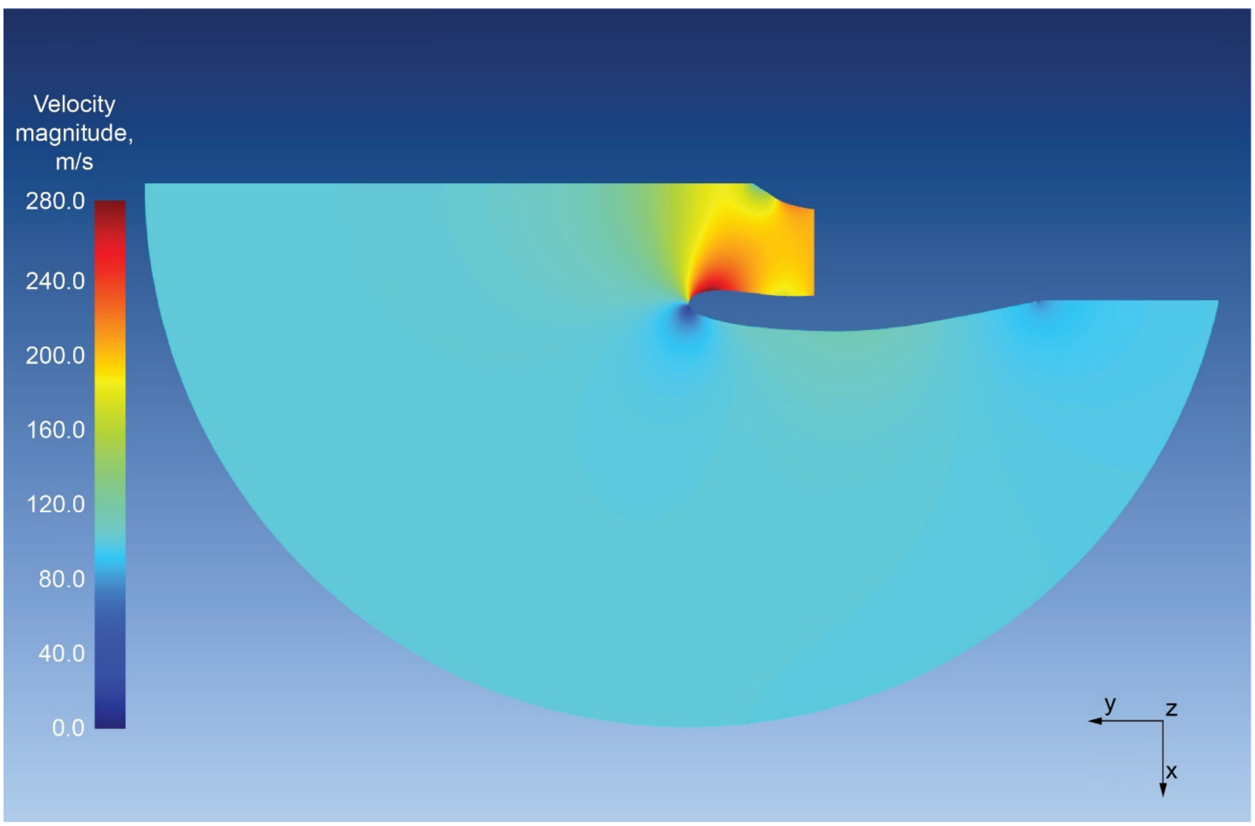

Figure 24.—Flow field for subsonic inlet with 200 m/s fan-face flow, 100 m/s external.

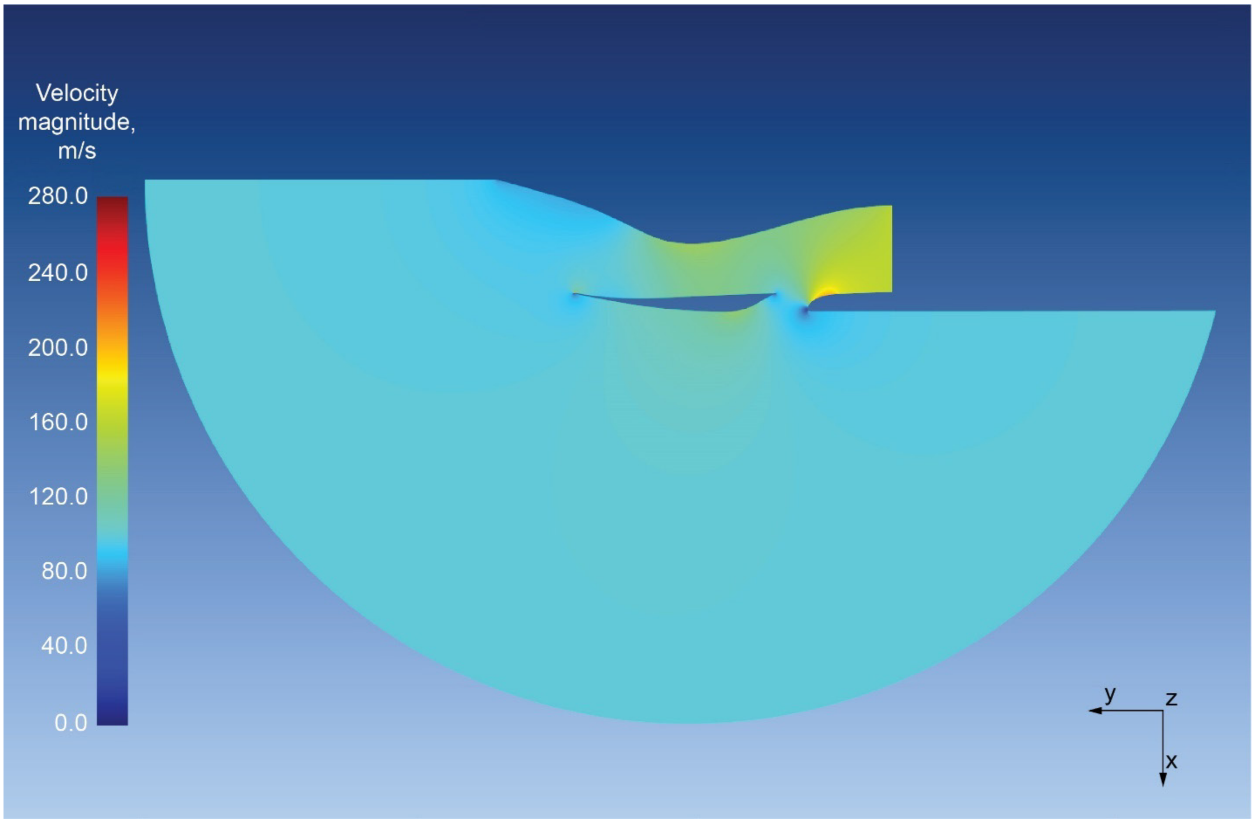

Figure 25.—Flow field for supersonic inlet with 160 m/s fan-face flow, 100 m/s external.

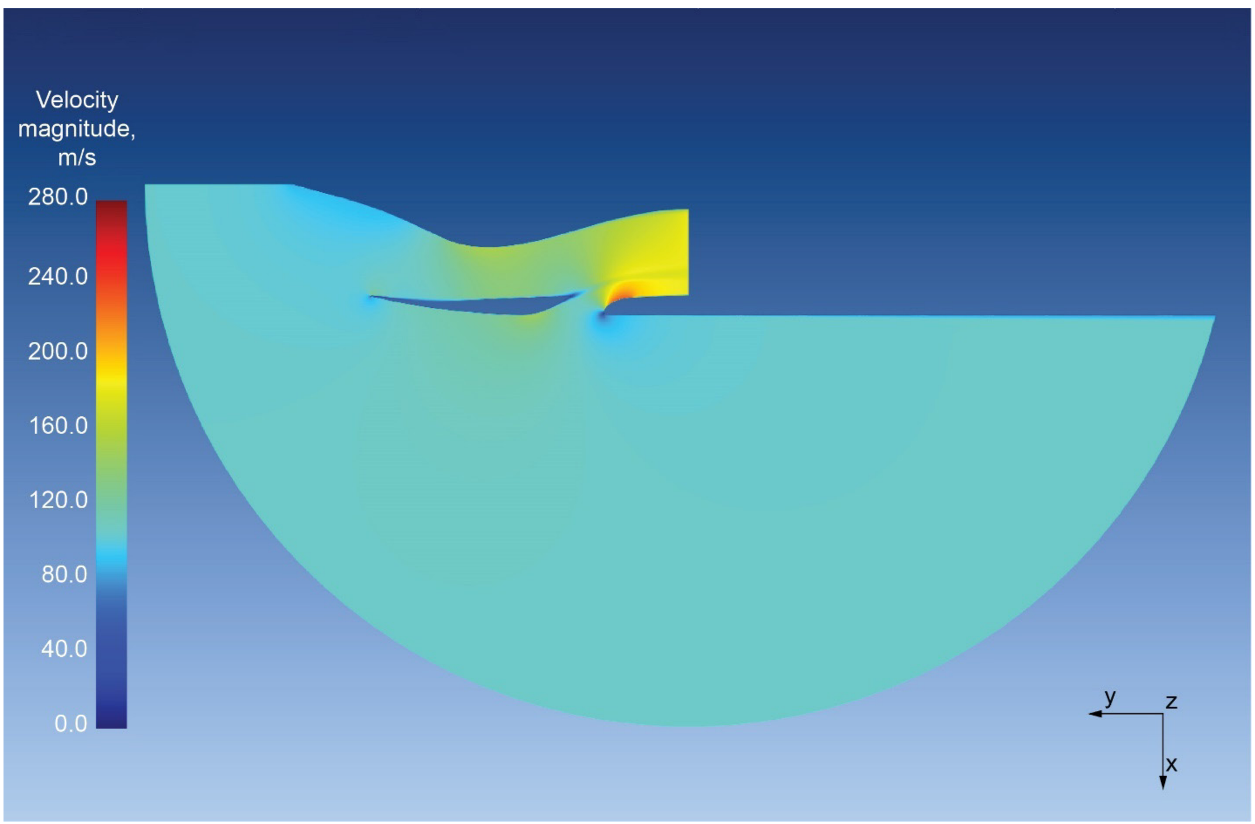

Figure 26.—Flow field for supersonic inlet with 200 m/s fan-face flow, 100 m/s external.

The same BPF tone and duct mode (2,080 Hz, m = 10, and n = 0) described previously was used for these results. Scripting in Python (Ref. 24) was used to facilitate the repeated modification of the boundary conditions and rerunning of Actran simulations. A sample of the acoustic fields is shown in Figure 27 to Figure 30.

The effect of fan-face Mach on acoustic directivity for the subsonic inlet is given in Figure 31. The peak amplitude of the main radiation lobe is affected by around 6 dB, along with a similar variation in level at broadside angles around 90°. The results are not monotonic, and no obvious patterns were identified. For example, the loudest downstream sound comes from the fastest case (200 m/s), while the lowest plotted is from the middle case (180 m/s).

The result using the supersonic inlet, shown in Figure 32, is even more difficult to interpret. This is understandable because both flow and sound fields are more complicated. A crude observation is that directivity shape and amplitude vary somewhat, but the effect on individual modes and frequencies cannot be easily summarized. One explanation is that there may be competing effects. As the fan-face flow velocity increases, the axial wavelength is compressed, and the propagation direction is closer to axial. Counteracting this effect, at the same time that the fan speed increases, the bubble of accelerated flow at the inlet highlight gets enhanced. This causes the spiraling waves to bend away from the axis.

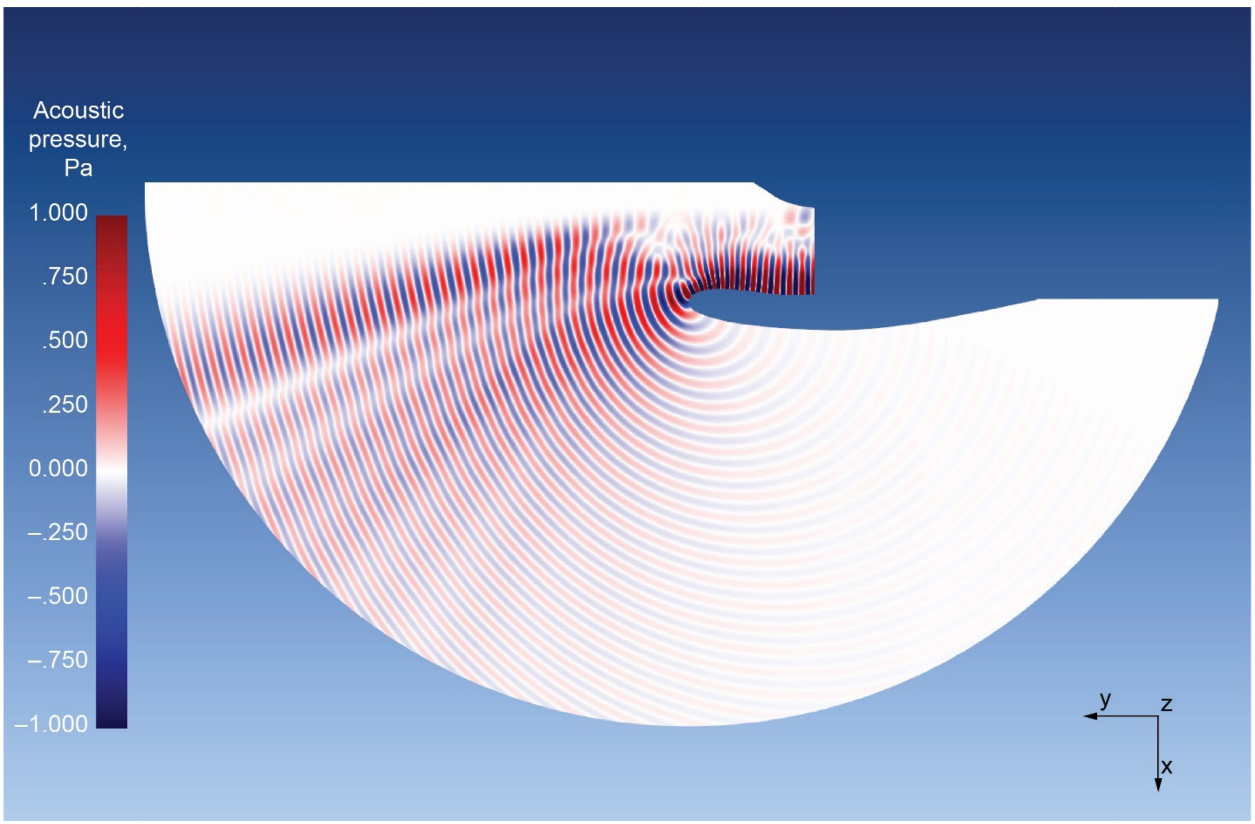

Figure 27.—Sound field for subsonic inlet with 160 m/s fan-face flow, 100 m/s external.

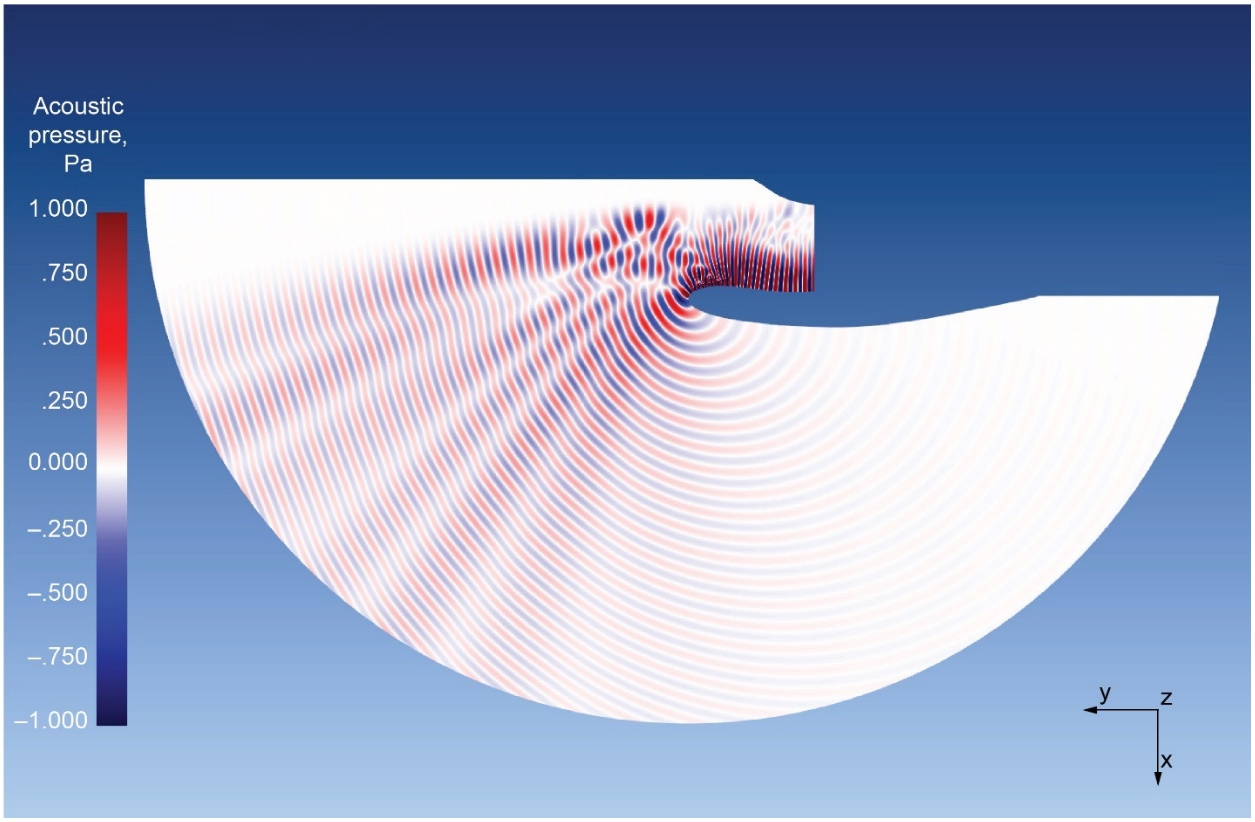

Figure 28.—Sound field for subsonic inlet with 200 m/s fan-face flow, 100 m/s external.

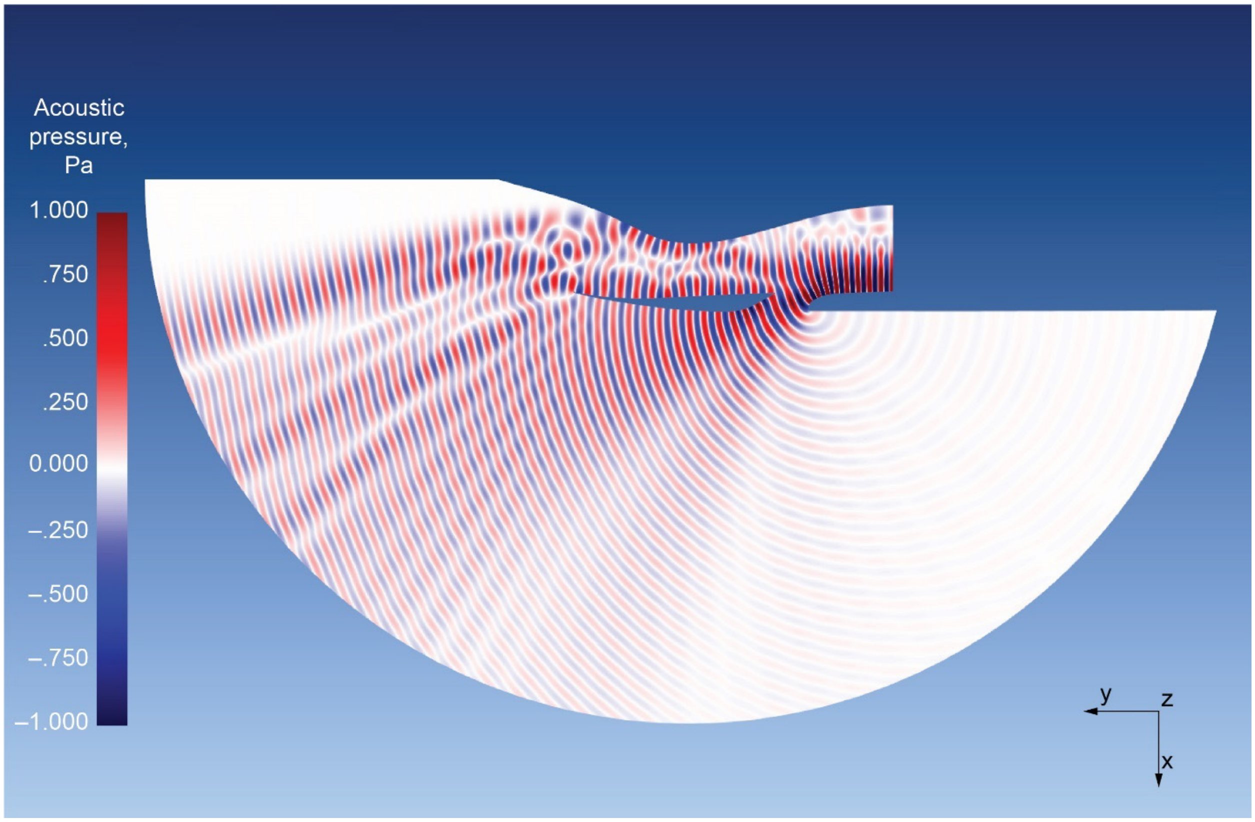

Figure 29.—Sound field for supersonic inlet with 160 m/s fan-face flow, 100 m/s external.

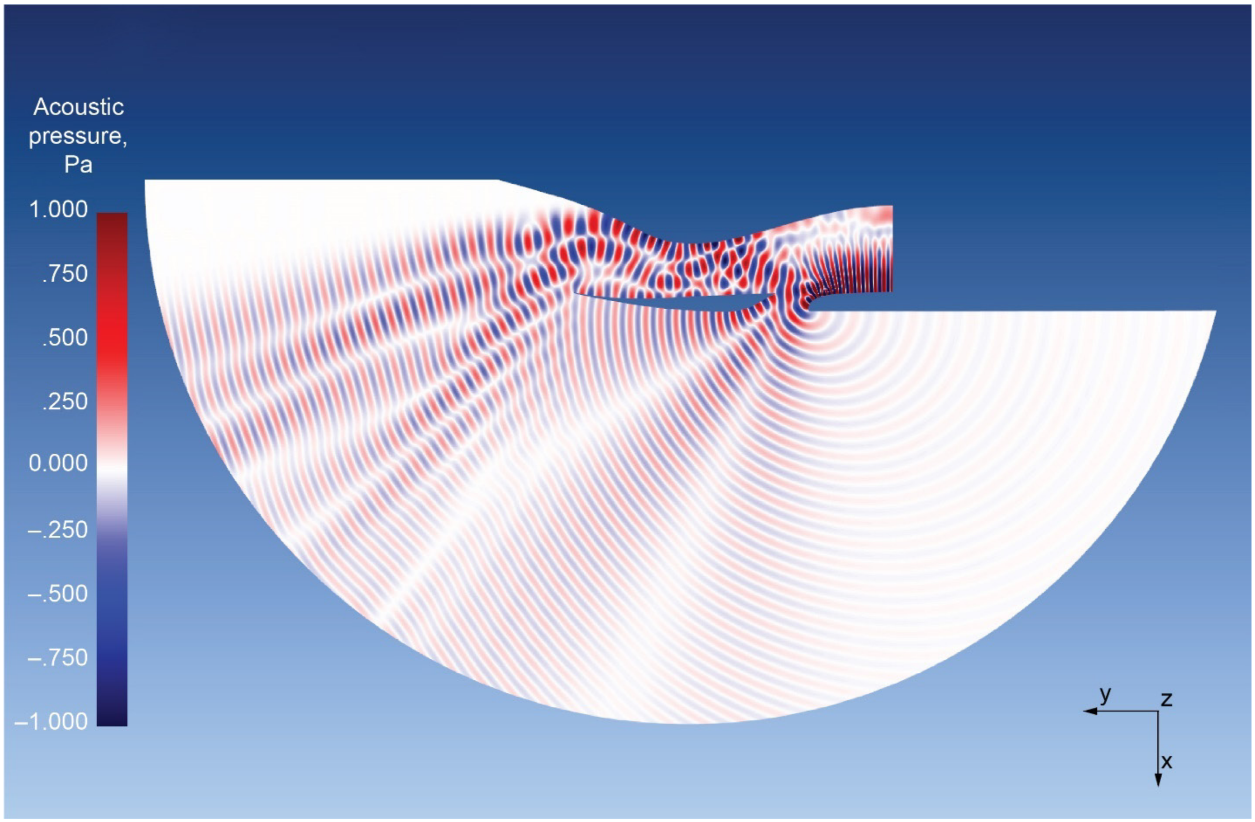

Figure 30.—Sound field for supersonic inlet with 200 m/s fan-face flow, 100 m/s external.

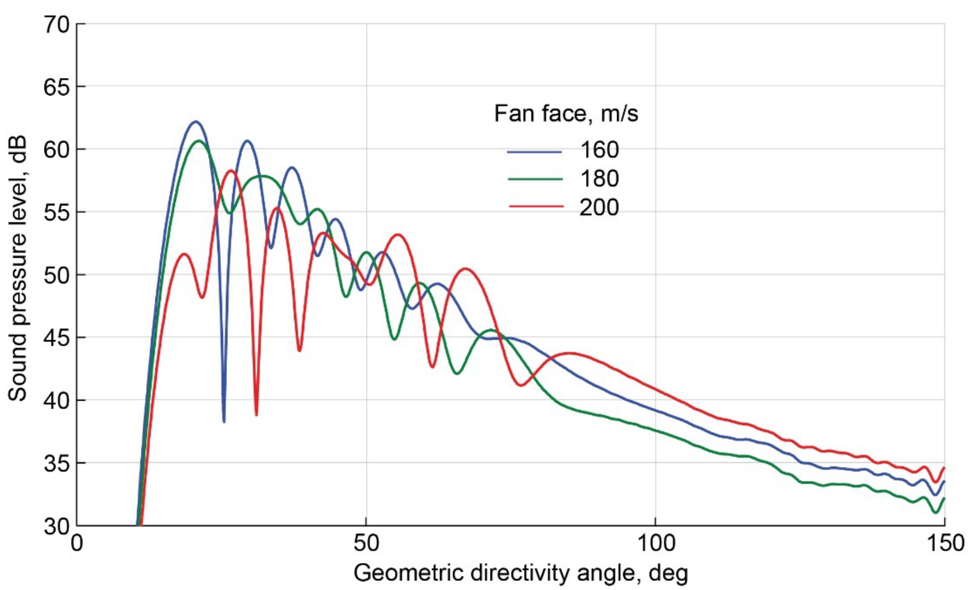

Figure 31.—Effect of fan-face speed on directivity for subsonic inlet.

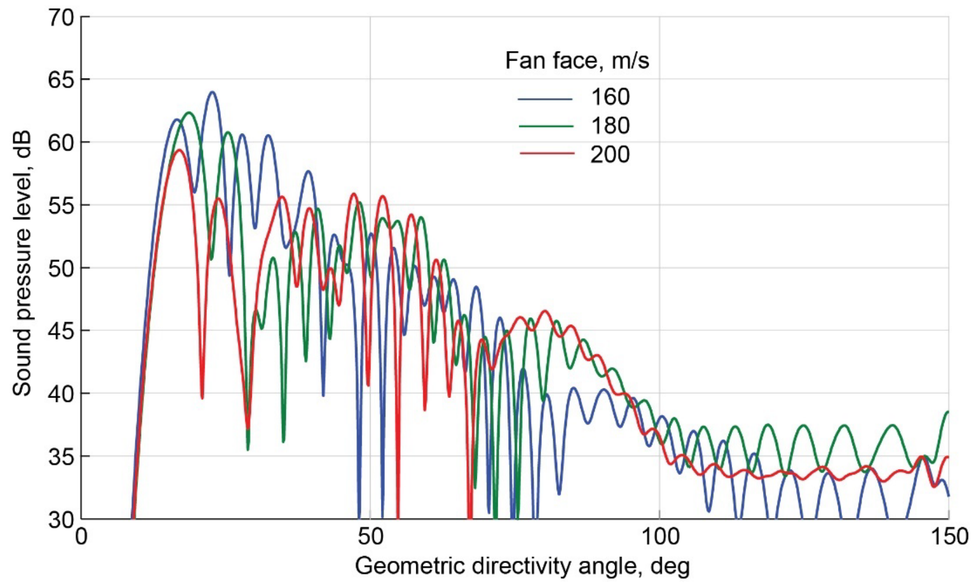

Figure 32.—Effect of fan-face speed on directivity for supersonic inlet.

4.2 Effect of Flow Solution

As mentioned in Section 3.0, the solution method makes several assumptions about the flow field. As an alternative to the inviscid compressible solver, a Reynolds-averaged Navier-Stokes (RANS) flow solution was computed using Ansys® Fluent, Release 20.2 (ANSYS, Inc.). Fluent code was run in axisymmetric mode with static pressure and free-stream values selected to achieve a Mach 0.30 free stream and Mach 0.53 fan face. A boundary layer mesh was used to achieve a boundary layer resolution of $y^+ \approx 1$ and the Shear Stress Transport (SST) turbulence model was used. The Ansys® flow solution was imported into Actran and interpolated to the acoustic domain with the recommended regularization steps. The RANS and inviscid results are given in Figure 33. Comparing the two flow solutions, it is apparent that the flow fields are substantially different, especially in the area of the auxiliary inlet slot and inlet throat. Note that this comparison was conducted with an earlier iteration of the geometry centered on the fan face.

The acoustic propagation solver was run with each of these flow fields, and the solutions were evaluated. Differences in the pressure map were found to be relatively difficult to distinguish visually and are not included. The resulting acoustic directivity at the field points is shown for each case in Figure 34, comparing the same 2,080 Hz, m = 10 duct mode propagating through the two different flow solutions for the LM1044 supersonic inlet. The upstream two lobes are nearly identical in both directivity and amplitude. The aft-radiated directivity is a bit lower in amplitude for the RANS simulation, but the trends are quite similar overall. All other solutions presented in the present report utilized the inviscid solver that is available in Actran.

4.3 Sound Power Propagation

The previous sections have focused on sound maps and the directivity pattern in the far field. This section focuses on sound power and considers whether, aside from ripples and interference patterns, the overall supersonic inlet noise radiation is meaningfully different than that of a subsonic inlet. In the limit of an auxiliary inlet with a very large axial gap, the upstream cowl and centerbody would have a small effect. The smooth curvature on the auxiliary inlet is qualitatively similar to that of the subsonic inlet lip. The two-port interference effect adds ripples to the directivity, but the overall propagation directions are similar, as seen in Figure 22.

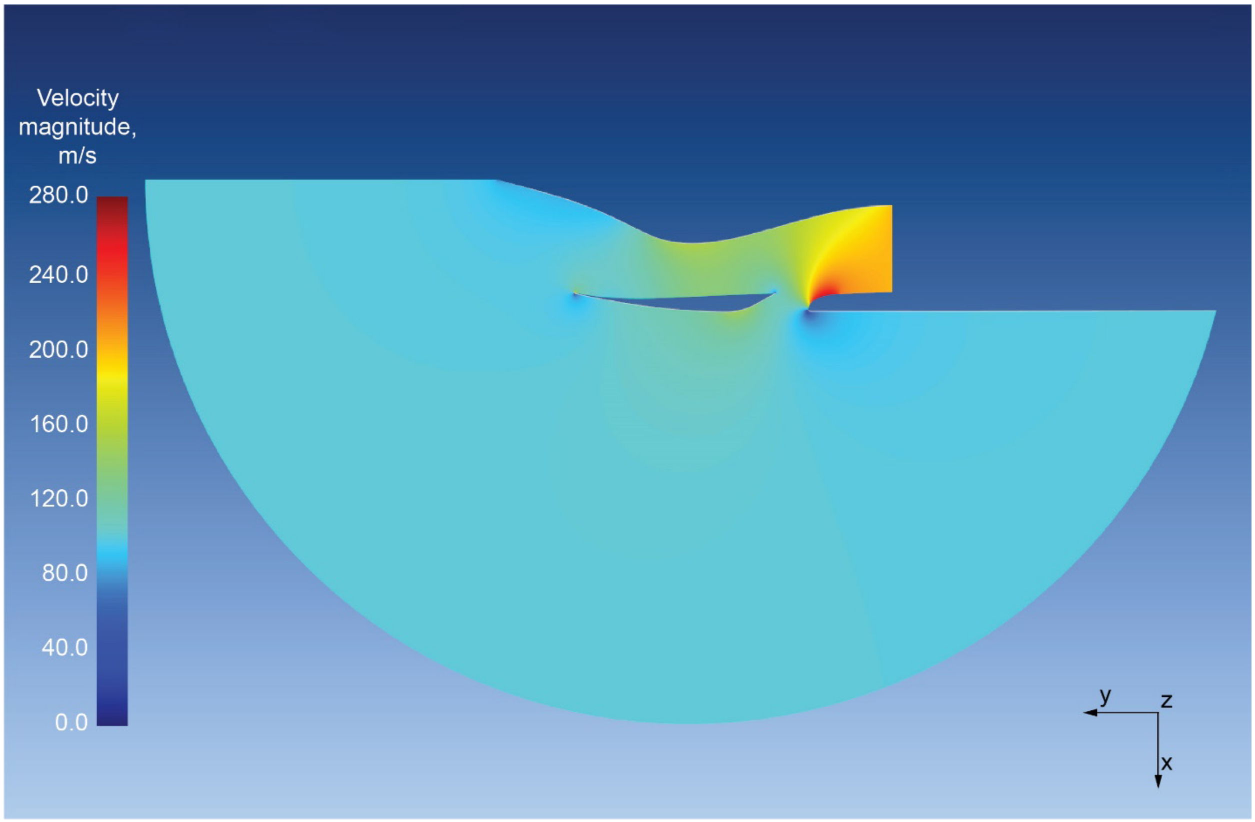

Figure 33.—Flow field for supersonic inlet computed using Reynolds-averaged Navier-Stokes (RANS) solver.

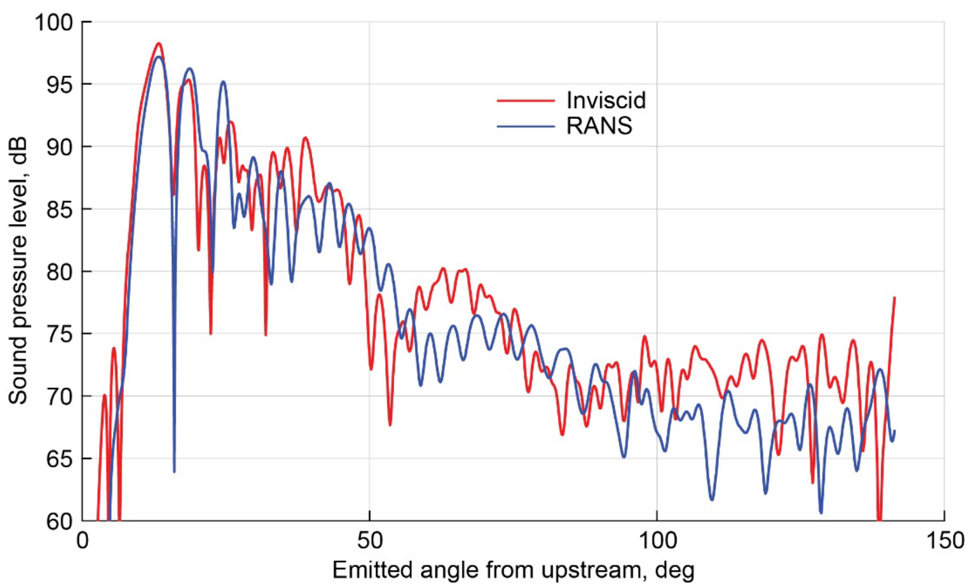

Figure 34.—Directivity showing effect of Reynolds-averaged Navier-Stokes (RANS) versus compressible potential flow field.

The metric of sound power can be convenient because it reduces a complicated sound field to a single number. For the supersonic inlet with auxiliary inlet, the sound power balance is as follows:

(a) Power is input at the fan-face plane.
(b) Power exits from the front inlet.
(c) Power exits from the auxiliary inlet.
(d) Power exits back into the fan face.
(e) Power radiates to the far field.

In the current simulations, all surfaces are hard (reflective), and there is no simulated damping by the air. Thus, the sound into the inlet must either exit from the front or auxiliary inlet or it can reflect back into the engine, (a) = (b) + (c) + (d). And the sound exiting the inlet from either inlet must then exit the domain, (e) = (b) + (c). This is illustrated in Figure 35. Note that the geometry is slightly different than the one used in other sections of this report.

Actran implements the method of Morfey (Ref. 25) for calculating the acoustic intensity in a flow field. To use this method, “lids” were created in the domain across the front and side inlet of the LM1044 geometry, as shown with dotted white lines in Figure 36. The intensity on these lids was exported and MATLAB® (The MathWorks, Inc.) was used to perform surface integral for acoustic power from intensity $\overline{I}$ as

$$\Pi = \int_S \overline{I} \cdot n dS \tag{2}$$

Actran also calculates the incident and reflected duct power, which was 2.03 and 0.01 W, respectively, for this case. The surface integral for the front and auxiliary inlets yields 0.77 and 1.26 W, respectively. This means 38 percent of the sound power exits the front inlet compared with 62 percent out the auxiliary inlet.

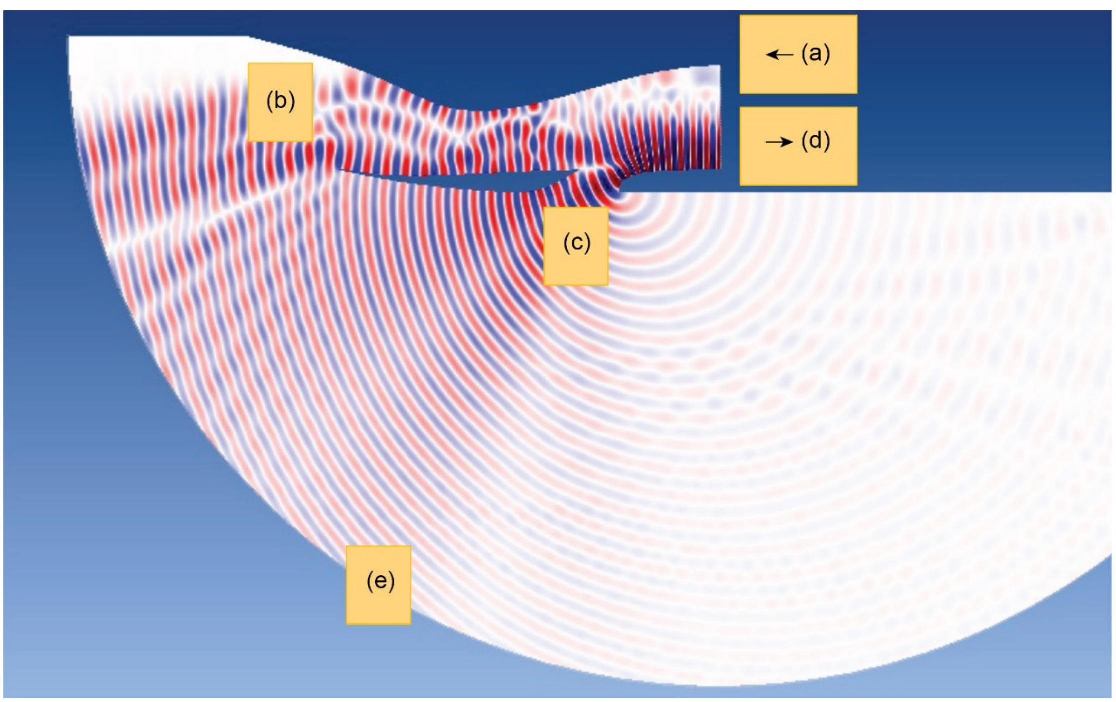

Figure 35.—Sound power balance example for supersonic inlet.

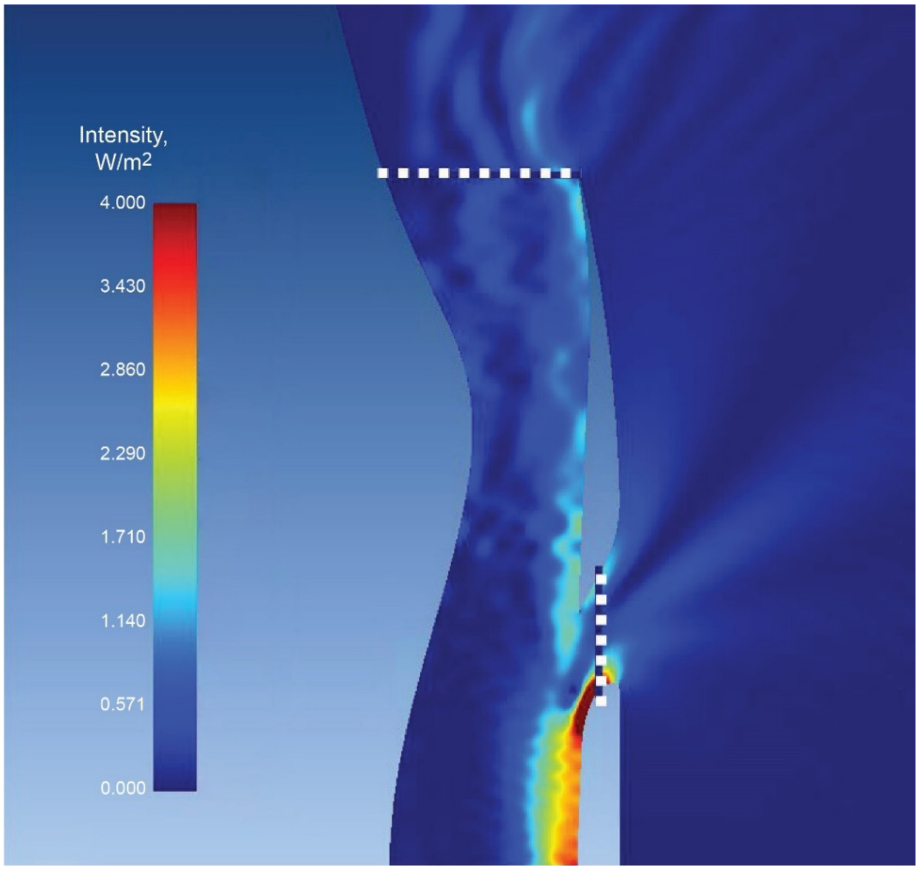

Figure 36.—Sound intensity map for supersonic inlet.

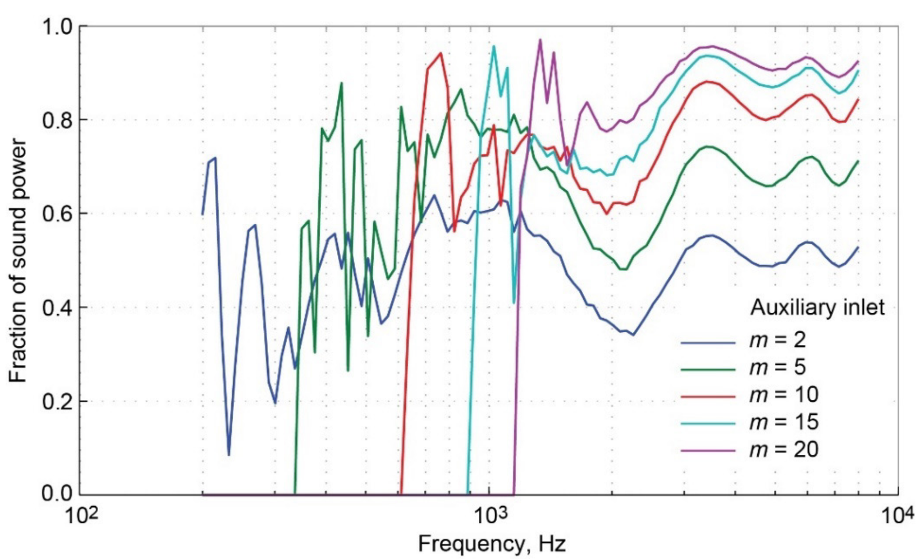

Figure 37.—Fraction of sound power exiting auxiliary inlet for various modes and frequencies. Azimuthal mode number (*m*).

Using more scripting, this calculation was repeated for a range of frequencies between 200 Hz and 8 kHz and azimuthal duct modes 2, 5, 10, 15, and 20, each with $n = 0$. The result is shown in Figure 37, represented as the fraction of the sound power that exits via the auxiliary inlet. Starting at the right side of the figure, it can be seen that there is a consistent pattern where the higher order modes propagate out the auxiliary inlet more readily in the limit of high frequency. At 8 kHz, 53 percent of the power propagates out the auxiliary inlet for $m = 2$, while 93 percent does for $m = 20$. When the duct mode first cuts on, it can also be seen to radiate strongly from the auxiliary inlet, reaching as high as 97 percent for $m = 20$ at 1,340 Hz.

4.4 Simulation Improvements

A few suggestions for improving the present simulations are provided. For the results shown, only one grid was used for each geometry, so it had to be sized for the highest frequency that would be studied. The simulations presented here took on the order of 10 min each for a single combination of geometry, frequency, and input mode. The simulations at lower frequency do not benefit from the finer grid, and the solver simply takes longer. Computational time can be reduced by using a coarser grid for lower frequencies. This will be of considerable importance if this work is extended to 3D geometries. Additionally, an automated method for sizing the acoustic grid based on the flow solution would allow a more elegant adaptation of the grid resolution to achieve the target number of points per convected wavelength. For the present work, the grid was refined manually in areas of high-speed flow.

Some peculiar sound maps were observed for the supersonic inlet at frequencies above 5 kHz, where a strong beaming of sound at angles around 90° was observed. These results were excluded from the present results since it was not clear if this effect was physical.

Extending the simulations to 3D would enable the incorporation of nonidealized auxiliary inlet geometry, such as an azimuthally segmented door, internal struts supporting the centerbody, and flow at an angle of attack to the inlet.

5.0 Correction Method

The investigations so far have focused on individual modes and frequencies. Since the correction is intended to be of general applicability, the simulation needed to be extended over a wide range of duct modes and frequencies. The grid was sized for solving frequencies up to 10 kHz, but seemingly unphysical results were observed above about 5 kHz, which was the upper frequency used for the results presented here. One hundred logarithmically spaced frequencies between 200 Hz and 10 kHz were used for running simulations. The modal content of the hypothetical engine is unknown, so a representative set of modes was used. Azimuthal orders from low to high were represented by $m = 2$, 4, 6, 10, and 20. The five lowest order radial modes were used. For reference, the $m = 2$ duct mode cuts on at 160 Hz, while $m = 10$ cuts on at 1,190 Hz. The frequency spacing between azimuthal cut-on frequencies is approximately 54 Hz for an annular duct of this size. No sensitivity to a particular mode has been identified, so the modes chosen were assumed to be a reasonable stand-in for other mode orders in this range.

The Actran TM direct frequency response method solves a single frequency at a time while preserving all phase information. This is an effective solution for a perfect pure tone where all constructive and destructive interference is included. The recommended workflow for computing broadband noise propagation from aircraft engine inlets is to solve multiple simulations for a given frequency, each a different duct mode excitation. The various solutions are assigned a random phase increment and summed, giving a pseudobroadband system response. This is the approach currently used, and the 25 modes applied are believed to be sufficient for a converged solution.

Figure 38 shows the directivity pattern as a contour plot. As mentioned, the lowest order (2,0) mode does not cut on until 160 Hz. The main radiation lobe can be seen moving further upstream as the frequency increases. Individual lobes can be identified for frequencies below around 2 kHz, at which point, the directivity is rather complicated in this representation. Compared to Figure 22, 25 modes are now applied to the inlet duct instead of only one.

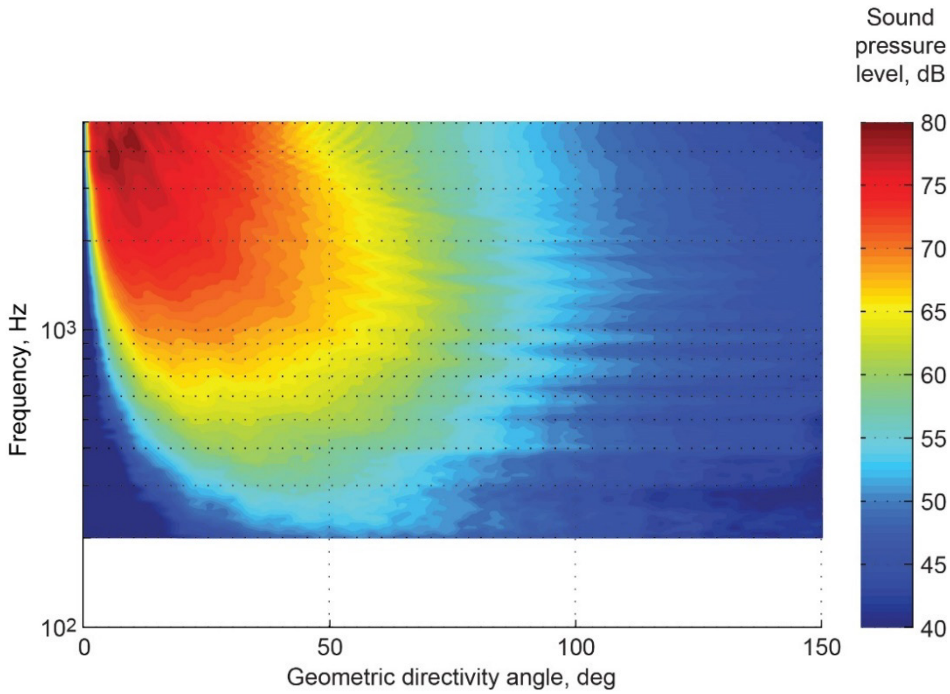

Figure 38.—Radiated sound directivity for subsonic inlet.

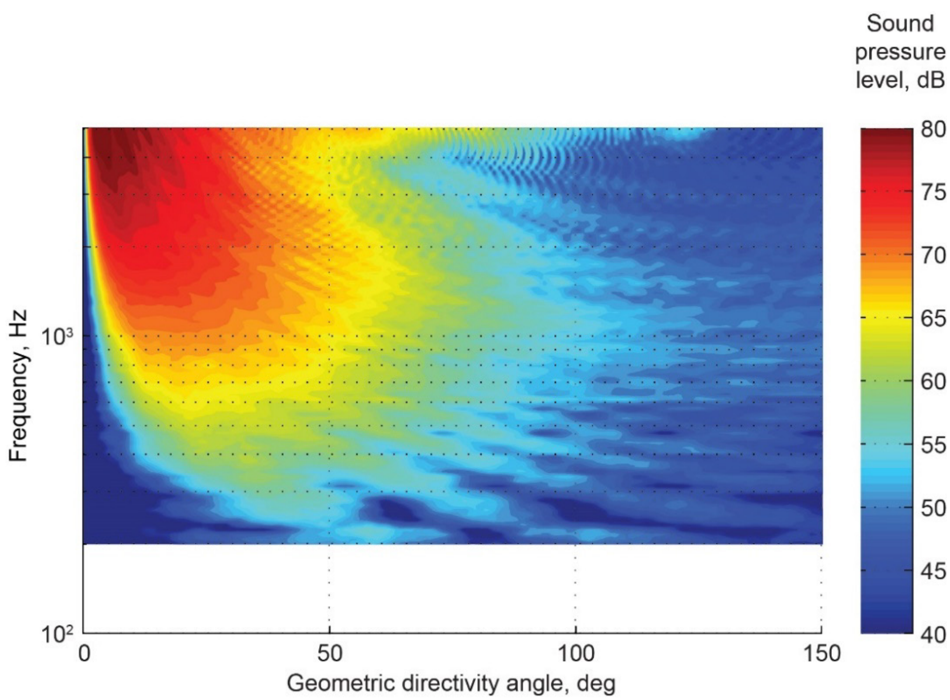

Figure 39.—Radiated sound directivity for supersonic inlet.

Figure 39 shows the result of the same modes applied to the supersonic inlet. Compared to the subsonic inlet, some of the directivity features are recognizable, such as the main lobes at frequencies below about 500 Hz. The many interference patterns are obvious, and it can be difficult to determine the effect of the inlet geometry by eye alone. The sound levels at angles between about 130° and 150° are higher for the supersonic inlet by perhaps 10 dB for frequencies above 2 kHz (upper right corner of the plot), suggesting more sound is being radiated aft.

A correction for inlet noise radiation can be represented as the subtraction of Figure 39 from Figure 38, giving Figure 40. The fan models operate on 10° increments and one-third octave band frequencies. Averaging the difference onto this coarser grid gives Figure 41.

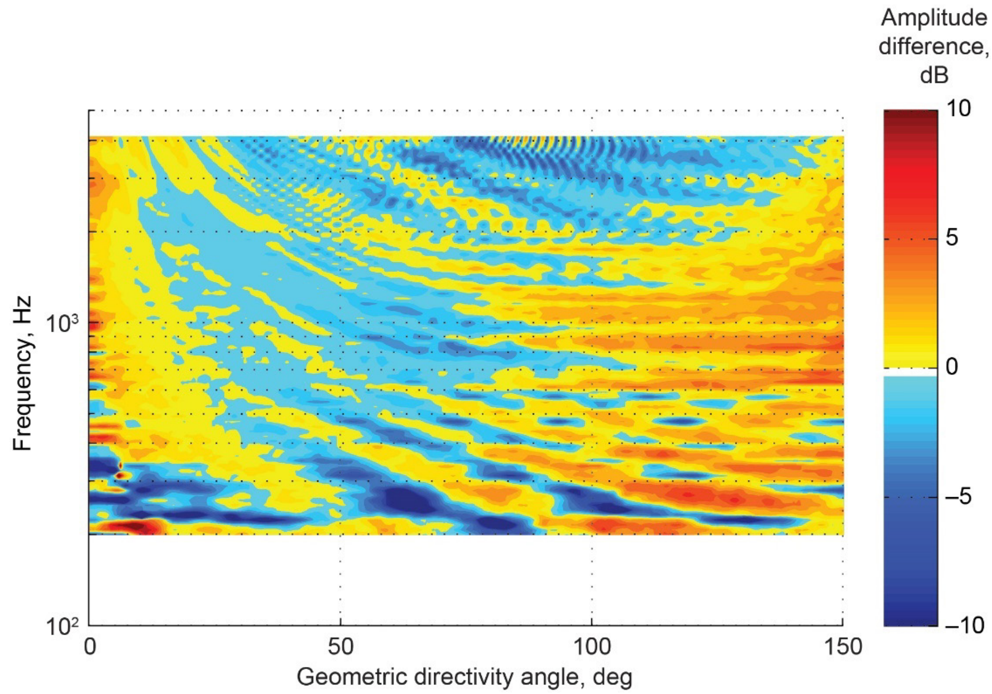

Figure 40.—Narrowband difference between inlet radiated noise from subsonic and supersonic inlets.

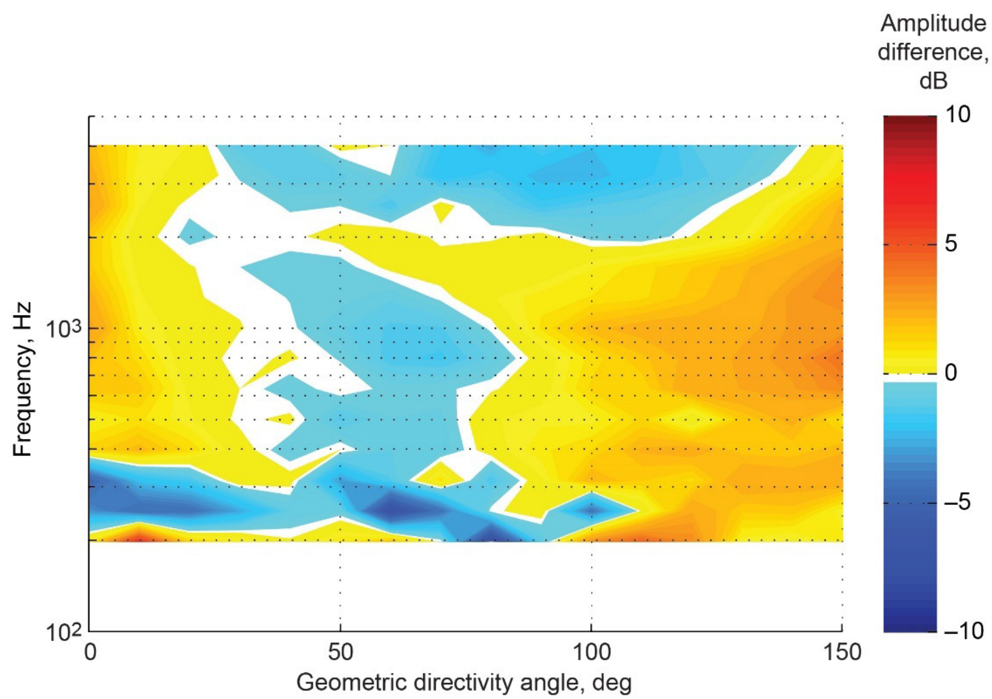

Figure 41.—Difference between inlet radiated noise from subsonic and supersonic inlets, averaged over 10° increments and one-third octave bands.

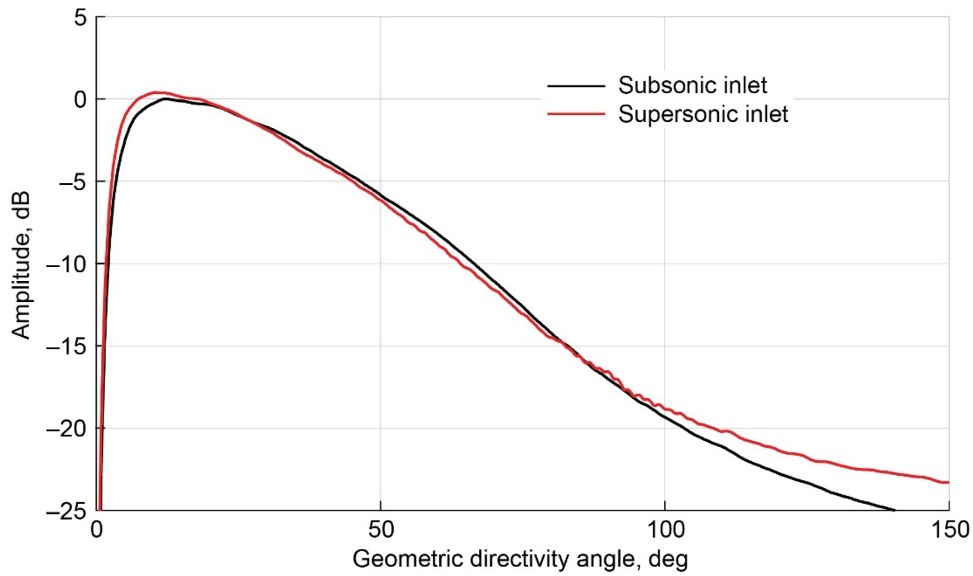

Figure 42.—Average directivity over all frequencies and modes tested.

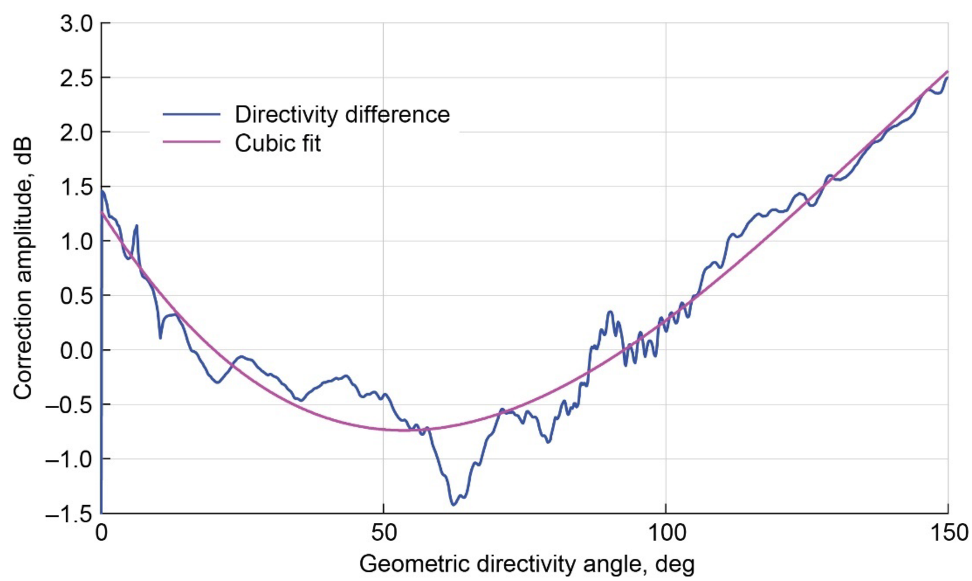

Figure 43.—Average directivity correction over all frequencies and modes tested.

Figure 42 shows the average of the two directivity patterns across all frequencies. This is not terribly rigorous, but since the existing fan models do not consider directivity as a function of frequency, it would not be meaningful to do so for this correction. This chart shows that the supersonic inlet directs more noise upstream of 10° and downstream of 100°.

Figure 43 shows the difference of the two directivity curves, such that the subsonic radiation pattern can be converted to better represent the supersonic radiation by adding this value as a “correction.” The cubic fit to the correction is

$$C_g = -2.28\times10^{-6}\,\theta_g^3 + 9.43\times10^{-4}\,\theta_g^2 - 0.0815\,\theta_g + 1.27 \tag{3}$$

where θ_g is the geometric angle in units of degrees, and C_g is the correction amplitude in decibels. Note that this expression and all the Actran simulations apply to the geometric directivity angle with a 100 m/s convecting flow with observers that are moving with the inlet. Depending on the user's specific application of the correction, it may need to be converted to a function of emitted directivity angle. The relationship between emitted angle θ_e and θ_g is given in Equation (4) as a function of Mach number M_0, which in this case is 0.294,

$$\theta_e = \theta_g - \arcsin(M_\theta \sin(\theta_g)) \tag{4}$$

Accounting for emitted angle,

$$C_e = -5.24\times10^{-6}\theta_e^3 + 1.50\times10^{-3}\theta_e^2 - 0.0994\theta_e + 1.16 \tag{5}$$

6.0 Effect on Flyover Noise

A simple implementation of the correction was conducted using existing fan models for inlet noise only. The fans and operating conditions come from a previous study on fan noise for a supersonic application (Ref. 11). The trajectory is a straight and level flyover at 305-m (1,000-ft) altitude at Mach 0.30 with three engines. Only inlet radiated BPF tone and broadband noise sources are included. Inlet MPTs and aft tone and broadband were turned off. The first fan is a single-stage design based on a 2.34-m- (92-in.-) diameter version of the Quiet High Speed Fan (QHSF) designed by Honeywell Engines and Systems. The tone-corrected perceived noise level flyover noise is shown in Figure 44, and it shows that the correction reduces the peak noise and redirects sound forward and aft. This effect is small, and the effective perceived noise level (EPNL) differs by less than 0.1 dB.

A similar effect is observed in Figure 45, where the simulated fan noise is from the F120 fan model from the HSRNoise program. A model two-stage fan was roughly used as a baseline and scaled up to a 1.65-m (65-in.) diameter. The effect on EPNL due to the correction is roughly 0.1 dB.

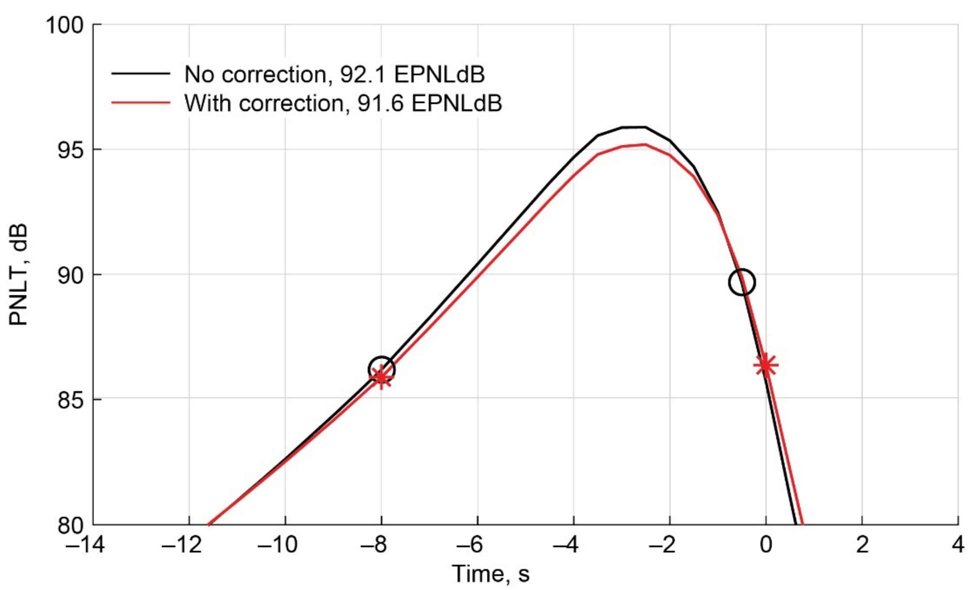

Figure 44.—Simulated flyover with Quiet High Speed Fan (QHSF) (Honeywell Engines and Systems) model parameters, with and without correction. Effective perceived noise level (EPNL). Tone-corrected perceived noise level (PNLT).

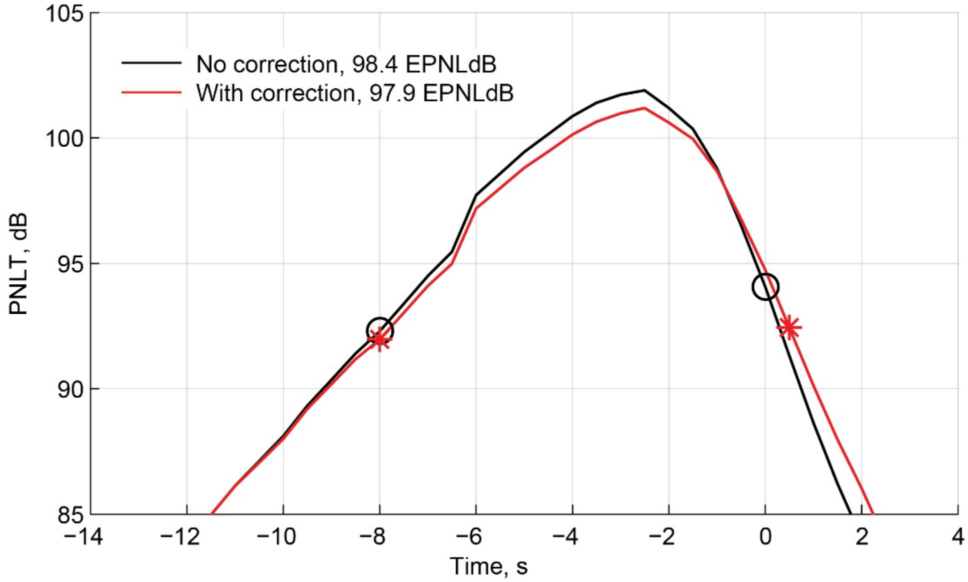

Figure 45.—Simulated flyover with F120 fan model parameters, with and without correction. Effective perceived noise level (EPNL). Tone-corrected perceived noise level (PNLT).

7.0 Conclusions

The noise radiating through a supersonic inlet has been investigated. Geometric and aerodynamic differences between subsonic and supersonic inlets were minimized, with identical duct diameters and flow conditions used. Acoustic simulations using Actran give the near-field radiated sound as well as far-field directivity. The axisymmetric method allows for full-scale computation of frequencies up to 5 kHz even in high-subsonic flows using a modest workstation. The method neglects viscous and shock effects, but inlets are designed to keep these conditions from occurring.

The supersonic inlet with auxiliary inlet door acts as an acoustic system with two sources at the same frequency, and this results in a pattern of constructive and destructive interference. The effects for an individual duct mode and frequency may be large at a particular point in the far field, but this effect is washed out when rolled up to a simulated flyover, and the quantitative difference to the effective perceived noise level (EPNL) was found to be small. The interpretation is that the duct modes input into the domain propagate at a certain angle, and the differences in the inlet geometry and flow field for the present study do not significantly alter the directivity.

References

1. Morgenstern, J., et al.: Advanced Concept Studies for Supersonic Commercial Transports Entering Service in the 2018–2020 Period Phase 2. NASA/CR—2015-218719, 2015. https://ntrs.nasa.gov
2. Heath, Christopher; Seidel, Jonathan; and Rallabhandi, Sriram K.: Viscous Aerodynamic Shape Optimization With Installed Propulsion Effects. AIAA 2017–3046, 2017.
3. Silcox, Richard J.: Geometry and Static Flow Effects on Acoustic Radiation From Ducts. AIAA J., vol. 22, no. 8, 1984, pp. 1087–1093.
4. Slater, John W.: SUPIN: A Computational Tool for Supersonic Inlet Design. AIAA 2016–0530, 2016.
5. Lopes, L.V.; and Burley, C.L.: ANOPP2 User's Manual: Version 1.2. NASA/TM—2016-219342, 2016. https://ntrs.nasa.gov

6. Heidmann, Marcus F.: Interim Prediction Method for Fan and Compressor Source Noise. NASA TM–X–71763, 1979. https://ntrs.nasa.gov
7. Hough, Joe W.; and Weir, Donald S.: Aircraft Noise Prediction Program (ANOPP) Fan Noise Prediction for Small Engines. NASA CR–198300, 1996. https://ntrs.nasa.gov
8. Kontos, K.B.; Janardan, B.A.; and Gliebe, P.R.: Improved NASA–ANOPP Noise Prediction Computer Code for Advanced Subsonic Propulsion Systems. NASA CR–195480, 1996. https://ntrs.nasa.gov
9. Krejsa, Eugene A.; and Stone, James R.: Enhanced Fan Noise Modeling for Turbofan Engines. NASA/CR—2014-218421, 2014. https://ntrs.nasa.gov
10. Sofrin, T.G.; and Pickett, G.F.: Multiple Pure Tone Noise Generated by Fans at Supersonic Tip Speeds. Pennsylvania State Univ. Fluid Mech., Acoustics, and Design of Turbomachinery, Pt. 2, 1974, pp. 435–459.
11. Stephens, David B.: Fan Noise for a Concept Commercial Supersonic Transport. AIAA 2017–4635, 2017.
12. Rawls, John W., Jr.; and Yeager, Jessie C.: High Speed Research Noise Prediction Code (HSRNOISE) User's and Theoretical Manual. NASA/CR—2004-213014, 2004. https://ntrs.nasa.gov
13. Ng, Wing: Comparison of the Aeroacoustics of Two Small-Scale Supersonic Inlets. NASA CR–96–206507, 1996. https://ntrs.nasa.gov
14. Li, S.-M.; Hanuska, C.A.; and Ng, W.R.: An Experimental Investigation of the Aeroacoustics of a Two-Dimensional Bifurcated Supersonic Inlet. J. Sound Vibration, vol. 248, no. 1, 2001, pp. 105–121.
15. Rice, Edward J.: Multimodal Far-Field Acoustic Radiation Pattern Using Mode Cutoff Ratio. AIAA J., vol. 16, no. 9, 1978, pp. 906–911.
16. Rice, E.; Heidmann, M.; and Sofrin, T.: Modal Propagation Angles in a Cylindrical Duct With Flow and Their Relation to Sound Radiation. NASA TM–79030, 1979. https://ntrs.nasa.gov
17. Eversman, Walter: Turbofan Acoustic Propagation and Radiation. Final Report, NASA NAG3–2109, 2000. https://ntrs.nasa.gov
18. Nallasamy, M.: Noise Radiation From Fan Inlet and Aft Ducts. AIAA 96–1769, 1996.
19. Han, Fei, et al.: Multiple Pure Tone Noise Prediction. J. Sound Vibration, vol. 333, no. 25, 2014, pp. 6942–6959.
20. Tyler, J.M.; and Sofrin, T.G.: Axial Flow Compressor Noise Studies. Tech. Rep., SAE Technical Paper 620532, 1962.
21. Free Field Technologies SA: ActranVI 2020 SP1 User's Guide. Vol. I, Installation, Operations, Theory and Utilities, 2020.
22. Mohring, Willi: A Well Posed Acoustic Analogy Based on a Moving Acoustic Medium. arXiv: 1009.3766, 2010.
23. Hughes, Christopher: Fan Noise Source Diagnostic Testrotor Alone Aerodynamic Performance Results. AIAA 2002–2426, 2002.
24. Van Rossum, Guido; and Drake, Fred L.: Python 3 Reference Manual. CreateSpace, Scotts Valley, CA, 2009.
25. Morfey, C.L.: Acoustic Energy in Non-Uniform Flows. J. Sound Vibration, vol. 14, no. 2, 1971, pp. 159–170.